

Manuscript Number: EPSL-D-17-01070R2

Title: Carbonate-platform response to the Toarcian Oceanic Anoxic Event in the southern hemisphere: Implications for climatic change and biotic platform demise

Article Type: Letters

Keywords: Toarcian Oceanic Anoxic Event; Tibetan Himalaya; Carbon isotopes; Storm deposits; Carbonate platform; Southern hemisphere.

Corresponding Author: Dr. Xiumian Hu, PhD

Corresponding Author's Institution: Nanjing University

First Author: Zhong Han

Order of Authors: Zhong Han; Xiumian Hu, PhD; David B. Kemp; Juan Li

Abstract: The Toarcian Oceanic Anoxic Event (T-OAE, ~183 Ma) was a profound short-term environmental perturbation associated with the large-scale release of  $^{13}\text{C}$ -depleted carbon into the global ocean-atmosphere system, which resulted in a significant negative carbon-isotope excursion (CIE). The general lack of characteristic T-OAE records outside of the northern hemisphere means that the precise environmental effects and significance of this event are uncertain. Many biotic carbonate platforms of the northern hemisphere western Tethys drowned or shifted to non-skeletal platforms during the early Toarcian. However, southern hemisphere records of Toarcian carbonate platforms are rare, and thus the extent and significance of biotic platform demise during the T-OAE is unclear. Here we present high-resolution geochemical and sedimentological data across two Pliensbachian-Toarcian shallow-water carbonate-platform sections exposed in the Tibetan Himalaya. These sections were located paleogeographically on the open southeastern tropical Tethyan margin in the southern hemisphere. The T-OAE in the Tibetan Himalaya is marked by a negative CIE in organic matter. Our sedimentological analysis of the two sections reveals an abundance of storm deposits within the T-OAE interval, which emphasizes a close link between warming and tropical storms during the T-OAE event, in line with evidence recently provided from western Tethyan sections of the northern hemisphere. In addition, our analysis also reveals extensive biotic carbonate-platform demise by drowning or changing to non-skeletal carbonates coincident with the onset of the CIE. Taken together, our results suggest that rapid and pervasive seawater warming in response to carbon release likely played a significant role in sudden biotic carbonate platform demise, and suppression/postponement of biotic platform re-development along the whole tropical/subtropical Tethyan margin.



南京大學  
**NANJING UNIVERSITY**

School of Earth Sciences and Engineering  
163 Xianlin Avenue, Nanjing, P. R. China  
Tel: 86 25 89683002 Fax: 86 25 83686016  
<http://www.nju.edu.cn>

February 10, 2018

Dear Editor Prof. Dr. Derek Vance:

We are very grateful to your and the reviewers' comments and suggestions on our manuscript entitled "Carbonate platform response to the Toarcian Oceanic Anoxic Event in the southern hemisphere: Implications for climatic change and biotic platform demise" (Manuscript NO.: EPSL-D-17-01070).

We have carefully addressed these very helpful comments and suggestions raised by the reviewer 1, and are returning the revised version of our manuscript to you as requested. We have highlighted the amendments in red in the revised manuscript.

Thanks for your careful review and effective handling of this manuscript.

We look forward to receiving your favorable reply. If you have any queries, please do not hesitate to contact me.

Yours sincerely,

Xiumian Hu

On behalf of the co-authors

Address:

Department of Earth Sciences and Engineering

Nanjing University

Nanjing, 210023, China

E-mail: [huxm@nju.edu.cn](mailto:huxm@nju.edu.cn)

Tel: 86-25-89683002

*Hu Xiumian*

## Response to editor and reviewers

Please could you attend to the very minor comments in Review 1 here and resubmit as soon as you can.

Thank you very much for processing our manuscript. The comments proposed by reviewer 1 have been carefully evaluated and all issues now addressed.

Reviewer #1: Han et al. have significantly revised their previous submission. The new version of the manuscript is better argued and punchier than the first two submissions, and the central argument of platform response to the T-OAE is now given better weighting over the much more ambiguous nuances of the C-isotope data. I believe that it is now ready for publication, pending some quite minor corrections.

We are grateful for your helpful comments and suggestions, and have carefully processed all remaining comments.

Line 24: change 'chemical type' to 'inorganic, non-skeletal carbonates...!'

We apologize for our imprecise wording. "Chemical type" has been rephrased throughout the revised manuscript as suggested.

Line 214-215: Clarify if you mean the relationship between different microfacies, or between  $\delta^{13}\text{C}_{\text{org}}$  and Ti.

Thanks for this suggestion. We have clearly stated that there is no clear relationship between microfacies and  $\delta^{13}\text{C}_{\text{org}}$ . Please see the modification in lines 215-216.

Line 216:  $\delta^{13}\text{C}_{\text{org}}$  is independent of detrital grain size...

We might have made a misunderstanding here by this sentence. Actually, we wanted to state that neither grain type and/or size (last sentence) nor detrital input (this sentence) influences the  $\delta^{13}\text{C}_{\text{org}}$  values. We apologize for this misunderstanding and have rephrased this sentence to avoid this. Please see the modification in lines 217-219.

Lines 218-220: This really needs to be phrased precisely and explicitly: %Ti is not a proxy for organic matter type, as is currently written. This isn't a problem, as long as they acknowledge the assumption they make, and problems associated with this assumption: that %Ti is a proxy for terrestrial organic matter flux, but that in many instances the relationship between the two parameters may not be linear and correlative (and thus should be taken as indicative, and not definitive evidence for mixing).

We apologize for our imprecise wording and have rephrased this sentence and surrounding sentences to make everything clearer. Please see the modification in lines 219-221.

Lines 239-240: The  $\delta^{34}\text{S}$  data at Yunjia is clearly problematic, so I am not clear why the authors choose to make a chemostratigraphic correlation via this section. At the moment, the correlation is made via C-isotopes to Yunjia; and then via S-isotopes to the Tethyan realm. Why not just go directly to the Tethys using the C-isotope data?

We thank the reviewer for bringing this to our attention. Using the C-isotope data to make a direct correlation is of course very important and we indeed did this (Figs. 6 and 7). We have therefore added a sentence at the beginning of section 5.2 to state this more clearly. The T-OAE has been only studied in the Yunjia section, ~500 m away from our studied Wölong section, but the age assignment was always somewhat ambiguous (Wignall et al., 2005; Newton et al., 2011). Therefore, it is warranted to make a chemostratigraphic correlation to make the age assignment clear through our new high-resolution data, coupled with a review of the biostratigraphic age constraints. Actually, we made the correlation between the Tibetan sections primarily on the top *Lithiotis* beds and associated flooding surfaces, as well as carbon isotopes of the Wölong section and sulfur isotopes of the Yunjia section (Fig. 4). Because the Wölong section shows the recovery trend of the T-OAE CIE, and the Yunjia section even does not show any CIE trend due to extreme low-resolution carbon isotopes, but presents a positive sulfur-isotope excursion, well coinciding with CIE in the Nianduo section. Therefore, on the basis of characteristic of *Lithiotis* bivalves, we use both the carbon- and sulfur- isotope correlations to define the age and draw the conclusion that the Pupuga–Nieniexiongla transition does indeed correspond to the onset of the T-OAE. Please see the modification in lines 232-235.

Line 263: semi-colon, not comma

Sorry for our previous mistake. Amended as suggested. Please see the modification in line 267.

Line 273: Insert 'difference' after 'this.'

Added as suggested. Please see the modification in line 277.

1 **Carbonate-platform response to the Toarcian Oceanic Anoxic Event in the southern**  
2 **hemisphere: Implications for climatic change and biotic platform demise**

3

4 **Zhong Han**<sup>1</sup>, **Xiumian Hu**<sup>1,\*</sup>, **David B. Kemp**<sup>2</sup>, **Juan Li**<sup>1</sup>

5

*1 State Key Laboratory of Mineral Deposit Research, School of Earth Sciences and Engineering,  
Nanjing University, Nanjing 210023, China*

*2 School of Geosciences, University of Aberdeen, Old Aberdeen AB24 3UE, U.K*

*\*Corresponding author: Dr. Xiumian Hu*

*E-mail: huxm@nju.edu.cn; Tel: 0086 25 89683002*

6 **Abstract**

7 The Toarcian Oceanic Anoxic Event (T-OAE, ~183 Ma) was a profound short-term  
8 environmental perturbation associated with the large-scale release of <sup>13</sup>C-depleted carbon into the  
9 global ocean-atmosphere system, which resulted in a significant negative carbon-isotope  
10 excursion (CIE). The general lack of characteristic T-OAE records outside of the northern  
11 hemisphere means that the precise environmental effects and significance of this event are  
12 uncertain. Many biotic carbonate platforms of the northern hemisphere western Tethys drowned or  
13 shifted to ~~chemical~~non-skeletal platforms during the early Toarcian. However, southern  
14 hemisphere records of Toarcian carbonate platforms are rare, and thus the extent and significance  
15 of biotic platform demise during the T-OAE is unclear. Here we present high-resolution

16 geochemical and sedimentological data across two Pliensbachian–Toarcian shallow-water  
17 carbonate-platform sections exposed in the Tibetan Himalaya. These sections were located  
18 paleogeographically on the open southeastern tropical Tethyan margin in the southern hemisphere.  
19 The T-OAE in the Tibetan Himalaya is marked by a negative CIE in organic matter. Our  
20 sedimentological analysis of the two sections reveals an abundance of storm deposits within the  
21 T-OAE interval, which emphasizes a close link between warming and tropical storms during the  
22 T-OAE event, in line with evidence recently provided from western Tethyan sections of the  
23 northern hemisphere. In addition, our analysis also reveals extensive biotic carbonate-platform  
24 demise by drowning or changing to ~~chemical-type~~non-skeletal carbonates coincident with the  
25 onset of the CIE. Taken together, our results suggest that rapid and pervasive seawater warming in  
26 response to carbon release likely played a significant role in sudden biotic carbonate platform  
27 demise, and suppression/postponement of biotic platform re-development along the whole  
28 tropical/subtropical Tethyan margin.

29 **Keywords:** Toarcian Oceanic Anoxic Event; Tibetan Himalaya; Carbon isotopes; Storm deposits;  
30 Carbonate platform; Southern hemisphere.

## 31 **1. Introduction**

32 The early Toarcian Oceanic Anoxic Event (T-OAE, ~183 Ma) was characterized by abrupt  
33 global warming, enhanced weathering rates, expansion of anoxic conditions, and the worldwide  
34 accumulation of organic-rich sediments (e.g., [Jenkyns, 1988, 2010](#); [Cohen et al., 2004](#); [Pearce et al., 2008](#);  
35 [Dera et al., 2011](#); [Brazier et al., 2015](#); [Fu et al., 2016](#)). It is characteristically marked by  
36 a negative carbon isotope ( $\delta^{13}\text{C}$ ) excursion (CIE) with an amplitude of ~3–8%, which typically  
37 interrupts a longer-term positive excursion attributable to the global increase in organic carbon

38 burial. The CIE has been recognised in bulk organic carbon, bulk carbonate, fossil wood and  
39 phytoclasts. In some studies, the shift to minimum  $\delta^{13}\text{C}$  values has been shown to occur in discrete,  
40 periodic steps (Kemp et al., 2005; Hesselbo et al., 2007; Hermoso et al., 2009, 2012; Hesselbo and  
41 Pieńkowski, 2011; Them et al., 2017). Two hypotheses have been put forward to explain the CIE:  
42 (i) methane hydrate dissociation from marine sediments and consequent release of  $^{12}\text{C}$  (e.g.,  
43 Hesselbo et al., 2000; Kemp et al., 2005); (ii) thermogenic emission of  $^{12}\text{C}$  induced by the  
44 intrusive emplacement of Karoo-Ferrar sills in organic-rich mudrocks (e.g., McElwain et al.,  
45 2005).

46 Although the T-OAE has been well documented in the western Tethys and Boreal realms (i.e.,  
47 Europe, e.g., Kemp et al., 2005; Hesselbo et al., 2007; Hermoso et al., 2009, 2012), fewer studies  
48 have been conducted elsewhere. Notable exceptions are recent studies from the NE Tethys (Fu et  
49 al., 2016), NW, central and NE Panthalassa (Caruthers et al., 2011; Gröcke et al., 2011; Kemp and  
50 Izumi, 2014), and the Sichuan Lake Basin, China (Xu et al., 2017). In the southern hemisphere,  
51 however, the T-OAE has been reported only from the Neuquén Basin, Argentina, which is a  
52 restricted back-arc rift basin formed during the Mesozoic (Al-Suwaidi et al., 2010, 2016).  
53 Therefore, no record of the T-OAE has been reported from an open-ocean setting in the southern  
54 hemisphere. Consequently, there is uncertainty as to whether the Toarcian CIE and corresponding  
55 environmental perturbations affected the southern hemisphere in the same way as the northern  
56 hemisphere. This has implications for assessing the severity, importance, and casual mechanism(s)  
57 of the event.

58 At the onset of the T-OAE, extensive demise of biotic carbonate platforms occurred in the  
59 western Tethys, attributed variously to the effects of falling carbonate production, tectonics,

60 eustasy, increased nutrient levels, or oceanic acidification (Woodfine et al., 2008; Lachkar et al.,  
61 2009; Merino-Tomé et al., 2012; Trecalli et al., 2012; Sabatino et al., 2013). However, the study of  
62 the relationship between the T-OAE and carbonate-platform evolution has thus far been restricted  
63 to the southern margins of western Tethys at low latitudes of the northern hemisphere.  
64 Consequently, only a localized understanding of carbonate-platform responses to the T-OAE has  
65 hitherto been gained, and the factors that triggered the demise of biotic platforms and delayed their  
66 recovery until well after the event are still uncertain and need to be better constrained.

67 In this paper, we present sedimentological and geochemical data across two uppermost  
68 Pliensbachian to lower Toarcian shallow-marine carbonate platform successions exposed in the  
69 Tibetan Himalaya, deposited at a low latitude ( $\approx 21.8^{\circ}\text{S}$  to  $\approx 26.1^{\circ}\text{S}$ ) in the southern hemisphere  
70 (Fig. 1A; Huang et al., 2015). We assess the environmental evolution of these platforms through  
71 the T-OAE, and discuss the possible global/regional factors controlling platform evolution and  
72 sedimentology along the Tethyan margin.

## 73 **2. Geological setting**

### 74 *2.1. Tectonic setting*

75 The Tethyan Himalayan Sequence, located between the Indus-Yarlung Zangbo Suture Zone  
76 to the north and the Greater Himalayan Sequence to the south (Fig. 1A and B; Gansser, 1964),  
77 consists mainly of Proterozoic to Eocene carbonate and siliciclastic sedimentary rocks that  
78 originally represented the northern margin deposits of the Indian subcontinent (Fig. 1D; Liu and  
79 Einsele, 1994; Jadoul et al., 1998; Sciunnach and Garzanti, 2012). This unit was traditionally  
80 subdivided into southern and northern zones. The southern zone is dominated by Lower Paleozoic



81 to Lower Eocene shallow-water carbonates and terrigenous rocks (Liu and Einsele, 1994; Jadoul  
82 et al., 1998; Sciunnach and Garzanti, 2012), whereas the northern zone is characterized by  
83 Mesozoic to Paleocene deep-water slope and rise sediments (Liu and Einsele, 1994). During the  
84 Early Jurassic, the Tethyan Himalaya migrated into the southern tropical/subtropical belt, and  
85 carbonate deposits gradually became extensive in the southern zone, forming the Kioto carbonate  
86 platform (Jadoul et al., 1998; Sciunnach and Garzanti, 2012; Huang et al., 2015).

## 87 2.2. Stratigraphy

88 The Nianduo section in the Nyalam area and the Wölong section in the Tingri area are  
89 located in the Tethyan Himalaya on the Kioto carbonate platform (Fig. 1B). Both sections have a  
90 continuously exposed marine sedimentary succession ranging from the upper Lower Jurassic  
91 Pupuga Formation to the lower Middle Jurassic Nieniexiongla Formation (Fig. 2A–D). The  
92 Pupuga Formation represents a shallow-water carbonate platform dominated by  
93 grainstones/packstones deposited under high-energy conditions with occasional influxes of  
94 terrigenous material. The lower-middle Pupuga Formation in both Tingri and Nyalam areas yields  
95 abundant and diversified benthic foraminifera including *Haurania deserta*, *Orbitopsella*  
96 *praecursor*, *Palaeomayncina termieri*, *Amijiella amiji*, *Cyclorbitopsella tibetica*, *Ammobaculites*  
97 *sp.*, *Lituosepta cf. compressa*, *Pseudocyclammina cf. liasica* (Jadoul et al., 1998; Wignall et al.,  
98 2006). These foraminiferal assemblages of the Tibetan Himalaya are similar to those observed in  
99 the Liassic carbonate platforms of the SW Tethyan margin in the northern hemisphere, and  
100 indicate a late Sinemurian–late Pliensbachian age (BouDagher-Fadel, 2008). In the upper Pupuga  
101 Formation, two intervals enriched in *Lithiotis* bivalves respectively occur ~20–30 m and ~3–4 m  
102 below the boundary with the overlying Nieniexiongla Formation in both the Nianduo and Wölong

103 sections (Figs. 3 and 4). *Lithiotis* bivalves are found in carbonate platforms throughout the tropical  
104 Tethys and Panthalassa, where they are limited to strata of late Pliensbachian to early Toarcian age  
105 (Fraser et al., 2004; Franceschi et al., 2014; Bodin et al., 2016). The overlying Nieniexiongla  
106 Formation represents a middle/outer carbonate ramp environment, and is characterized by  
107 mudstones deposited under low-energy conditions intercalated with abundant coarse-grained beds  
108 (Han et al., 2016). In the lower Nieniexiongla Formation, ammonites (*Polyplectus discoides*,  
109 *Dumortieria* sp., *Phymatoceras* cf. *crasstcosta*) collected in thin-bedded mudstones near the  
110 Nianduo section were assigned to the *bifrons-levesquei* zones of the middle-late Toarcian (Fig. 3;  
111 Yin, 2010). The upper part of this unit in the Wölong section yields ammonites (*Leptosphinctes*  
112 sp.) suggestive of a Bajocian age (Jadoul et al., 1998). In addition to these biostratigraphic  
113 constraints, further important information on the age of the studied stratigraphy can be derived  
114 from available stable sulfur isotope ( $\delta^{34}\text{S}$ ) stratigraphy (Newton et al., 2011). Based on the *lituolid*  
115 foraminifera and *Lithiotis* bivalves, the studied sections can be readily correlated with the nearby  
116 Yunjia section (~500 m away from the Wölong section, Fig. 1C). Newton et al. (2011) suggested  
117 that a marked shift in  $\delta^{34}\text{S}$  data in the Yunjia section close to the Pupuga–Nieniexiongla boundary  
118 can be correlated with a similar shift in the biostratigraphically well-constrained Yorkshire (UK)  
119 section. Based on this correlation, the Pupuga–Nieniexiongla transitional interval is most probably  
120 coeval with the upper *tenuicostatum*-lower *falciferum* ammonite Zone boundary in Europe, and  
121 thus of early Toarcian age.

### 122 3. Material and Methods

123 Rock samples were collected from the Nianduo section (28°40'52"N, 86°08'7"E) of Nyalam  
124 County and the Wölong section (28°29'2"N, 87°02'3"E) of Tingri County in the Tibetan Himalaya

125 (Fig. 1B and C). Samples were collected with an average spacing of 1 m, reduced to ~0.2–0.3 m in  
126 the Nianduo section and 0.1–0.2 m in the Wölong section across the Pupuga–Nieniexiongla  
127 stratigraphic transition.

128 A total of ~~131~~132 samples from the Nianduo section and 124 samples from the Wölong  
129 section were analyzed for organic carbon-isotope composition ( $\delta^{13}\text{C}_{\text{org}}$ ) at the SINOPEC Wuxi  
130 Research Institute of Petroleum Geology. Powdered samples were treated with 2N HCl at 80°C for  
131 at least 3 hours to remove carbonate, and were then washed with distilled water to remove residual  
132 HCl. Organic carbon-isotope analyses were performed on dried samples using a Finnigan MAT  
133 253 mass spectrometer, with an instrumental standard deviation of  $\pm 0.1\%$ . Isotopic measurements  
134 were calibrated to Chinese national standard charcoal sample GBW04407 ( $\delta^{13}\text{C}_{\text{VPDB}} = -22.43\% \pm$   
135  $0.07\%$ ). Results were reported in standard  $\delta$ -notation relative to the Vienna Peedee Belemnite  
136 (VPDB) standard. To supplement our  $\delta^{13}\text{C}_{\text{org}}$  data,  $\delta^{13}\text{C}$  and  $\delta^{18}\text{O}$  of bulk carbonate were measured  
137 on 98 samples across the Pupuga–Nieniexiongla boundary interval in the Nianduo section using a  
138 Finnigan MAT 252 isotope ratio mass spectrometer at the State Key Laboratory of Marine  
139 Geology at Tongji University. The isotope results of  $\delta^{13}\text{C}_{\text{carb}}$  and  $\delta^{18}\text{O}_{\text{carb}}$  were corrected to VPDB  
140 standard, with analytical uncertainties of  $\pm 0.06\%$  and  $\pm 0.08\%$ , respectively.

141 Total organic carbon (TOC) analysis was performed on 69 samples, parallel to the  $\delta^{13}\text{C}_{\text{carb}}$   
142 samples, across the Pupuga–Nieniexiongla boundary interval in the Nianduo section using a Vario  
143 Cube CN elemental analyzer (Elementar, Germany) at the State Key Laboratory of Marine  
144 Geology of Tongji University. Prior to analysis, these samples were treated with 10% HCl for at  
145 least 24 h to remove inorganic carbon. Titanium concentrations was determined on 53 powdered  
146 samples from the Nianduo section using an Olympus Delta Premium handheld XRF (hhXRF)

147 instrument at the University of Aberdeen. The calibration ~~errors (uncertainties) and reproducibility~~  
148 ~~for error (uncertainty) of Ti were measurements is~~ better than 0.025% ~~and 0.4%. Reproducibility,~~  
149 ~~based on repeat measurement of a standard, was better than 0.009% (1 s.d., 2.36%, respectively, %~~  
150 ~~relative s.d.).~~

## 151 4. Results

### 152 4.1. Geochemical data

#### 153 4.1.1. Isotope geochemistry

154 Carbon- and oxygen-isotope data are plotted stratigraphically in Fig. 3 for the Nianduo  
155 section and in Fig. 4 for the Wölong section. In the Nianduo section, a negative CIE of  $\sim -2.5\text{‰}$  is  
156 recorded in organic matter ( $-0.3$  to  $28.4$  m; Fig. 3). This CIE starts at the topmost Pupuga  
157 Formation, just above the top of the *Lithotis*-rich interval.  $\delta^{13}\text{C}_{\text{org}}$  values are variable between  
158  $-0.3$  m and  $\sim 16$  m during the overall shift to minimum values.  $\delta^{13}\text{C}_{\text{carb}}$  data primarily range  
159 between  $1\text{‰}$  and  $2.5\text{‰}$ , and show an overall negative trend beginning shortly after the  
160 Pupuga–Nieniexiongla boundary ( $\sim 0$  m) and extending to  $\sim 30$  m, with a small magnitude of  
161  $\sim -1.5\text{‰}$ . However,  $\delta^{13}\text{C}_{\text{carb}}$  data do not show the same profile as the  $\delta^{13}\text{C}_{\text{org}}$  data (Fig. 3). The  
162 corresponding oxygen-isotope data mainly range from  $-8$  to  $-5\text{‰}$ , with an average value of  
163  $-6.4\text{‰}$ .

164 Compared to the Nianduo section,  $\delta^{13}\text{C}_{\text{org}}$  data in the Wölong section do not show a  
165 decreasing trend close to the Pupuga–Nieniexiongla boundary (Fig. 4). A broad negative CIE of  
166  $\sim -2.5\text{‰}$  is, however, apparent higher up in the section between  $\sim 8$  m and  $\sim 30$  m. The recovery  
167 profile of this excursion between  $\sim 15$  m and  $\sim 30$  m is similar to the recovery profile of the  $\delta^{13}\text{C}_{\text{org}}$

168 data between ~15 m and ~30 m in the Nianduo section.

#### 169 4.1.2. TOC and elemental content

170 TOC values from the Nianduo section range from 0.05 to 0.3 wt.%, with an average value of  
171 0.14 wt.% (Fig. 3). An increase in TOC values occurs shortly after the onset of the CIE between  
172 ~0 m and ~8 m. Ti abundance in the Nianduo section is plotted in Fig. 3 and primarily ranges  
173 between 0.05% and 0.15%, with an average value of 0.069%.

#### 174 4.2. Sedimentological observations

175 As noted above, and previously by Han et al. (2016), platform-top grainstones deposited  
176 under high-energy conditions of the Pupuga Formation are abruptly overlain by middle/outer ramp  
177 mudstones reflecting low-energy conditions of the Nieniexiongla Formation in the Nianduo and  
178 Wölong sections (0 m datum in both sections). The interval immediately above this flooding  
179 surface in both the Nianduo and Wölong sections is characterized by the common occurrence of  
180 coarse-grained beds, e.g., rudstones, floatstones, siltstones, oolitic grainstones, and peloidal  
181 packstones/wackestones (Han et al., 2016; Figs. 3 and 4). These intervals show abundant and  
182 diverse sedimentary structures such as wave ripples (Fig. 2E) and small-scale hummocky and  
183 swaley cross-stratification (HCS and SCS; Fig. 2F). Some sandy beds within mudstones show  
184 weak HCS individually (Fig. 2G) or just above the U/V-shaped gutter casts (Fig. 2H). In addition,  
185 other sedimentary structures, e.g., parallel laminations, climbing ripples, graded bedding and sharp  
186 erosive bases, are also readily observed both at outcrop and in microfacies (Han et al., 2016).  
187 These coarse-grained beds and related structures are particularly concentrated in the Nianduo  
188 section between ~0 m and ~12 m, coincident with the overall shift to minimum  $\delta^{13}\text{C}_{\text{org}}$  values. In

189 the Wölong section, they are also concentrated close to the base of the Nieniexionglia Formation.

## 190 5. Discussion

### 191 5.1. Diagenetic and source effects on carbon-isotope data

192 The early Toarcian negative CIE has been widely recorded in a range of marine environments,  
193 including shallow-water carbonate platforms (e.g., Kemp et al., 2005, Hesselbo et al., 2007,  
194 Woodfine et al., 2008; Trecalli et al., 2012; Sabatino et al., 2013; Them et al., 2017). However,  
195 high-energy deposits on shallow-water platforms are readily influenced by freshwater diagenesis  
196 or organic matter source changes (Oehlert and Swart, 2014; Suan et al., 2015). The measured  $\delta^{18}\text{O}$   
197 values ( $>-10\text{‰}$ ) in the Nianduo section, coupled with the absence of any correlation between  $\delta^{18}\text{O}$   
198 and  $\delta^{13}\text{C}_{\text{carb}}$  ( $R^2=0.005$ , Fig. 5A), suggests limited diagenetic influence on the  $\delta^{13}\text{C}_{\text{carb}}$  data (Brasier  
199 et al., 1990; Kaufman and Knoll, 1995). The decoupled  $\delta^{13}\text{C}_{\text{org}}$  and  $\delta^{13}\text{C}_{\text{carb}}$  relationship ( $R^2=0.023$ ,  
200 Fig. 5B) possibly indicates evidence for diagenetic alteration (e.g., Knoll et al., 1986, see also,  
201 however, Oehlert and Swart, 2014). Nevertheless, the overall pattern of  $\delta^{13}\text{C}_{\text{org}}$  changes in the  
202 Nianduo section is comparable to that recognized from well-preserved T-OAE successions  
203 elsewhere (e.g., Kemp et al., 2005; Hesselbo et al., 2007; Hermoso et al., 2009, 2012; Sabatino et  
204 al., 2013, see discussion below), albeit with lower magnitude variations (Figs. 6 and 7). The range  
205 of  $\delta^{13}\text{C}_{\text{org}}$  values from the Nianduo section broadly correspond to the coeval range known from the  
206 western Tethyan Apennine and High Atlas platforms (Trecalli et al., 2012; Bodin et al., 2016).  
207 Taken together, therefore, these observations suggest that the  $\delta^{13}\text{C}_{\text{org}}$  signal from the Nianduo  
208 section is not significantly modified by diagenesis.

209 Given the abrupt facies change and appearance of coarse grained siliciclastic-rich beds at the

210 upper Pupuga Formation to lower Nienixiongla Formation boundary, we consider the possible  
211 influence of organic-matter source changes on our  $\delta^{13}\text{C}_{\text{org}}$  data caused by microfacies variations  
212 and terrestrial input. To do this, we divided the lithologies of the Nianduo and Wölong sections  
213 into four characteristic microfacies based on grain type and/or size (Figs. 3 and 4).  $\delta^{13}\text{C}_{\text{org}}$  data  
214 from each microfacies are shown on the stratigraphic log for the two sections (Figs. 3 and 4). In  
215 addition, Fig. 5C shows cross-plots between  $\delta^{13}\text{C}_{\text{org}}$  from each microfacies in the Nianduo section  
216 and Ti, ~~an established~~ proxy for detrital input (e.g., Kemp and Izumi, 2014). The data indicate  
217 that each microfacies type has a wide range of  $\delta^{13}\text{C}_{\text{org}}$  values, and there is no clear relationship  
218 between ~~them microfacies and~~  $\delta^{13}\text{C}_{\text{org}}$ . Thus, the  $\delta^{13}\text{C}_{\text{org}}$  values from the Tibetan sections are  
219 independent of changes of grain type and/or size. ~~Equally~~ Overall,  $\delta^{13}\text{C}_{\text{org}}$  varies independently of  
220 Ti for each microfacies. ~~Microfacies, and although microfacies~~ 3 is typically associated with high  
221 Ti values (Fig. 5C), ~~but~~  $\delta^{13}\text{C}_{\text{org}}$  values of microfacies 3 are variable and show no correlation with  
222 Ti. These observations further suggest that changes in detrital input, and thus possible changes in  
223 terrestrial organic matter flux, ~~overall has~~ likely have a negligible influence on the observed  
224 changes in  $\delta^{13}\text{C}_{\text{org}}$  in the Nianduo section. Nevertheless, we note that 6 samples with anomalously  
225 high  $\delta^{13}\text{C}_{\text{org}}$  values at ~10 m height in the Nianduo section come predominantly from an interval  
226 of enhanced ~~terrestrial~~ detrital input, as indicated by higher Ti values (Fig. 3). This observation  
227 may be ascribed to the fact that these specific samples have the most significant terrigenous  
228 influence, and are thus potentially more readily affected by organic matter source change, i.e.,  
229 compositional mixing. Indeed,  $\delta^{13}\text{C}_{\text{org}}$  in both sections may be sensitive to organic matter source  
230 changes given the conditions of extremely low TOC values (typically <<1%, Fig. 3). Therefore,  
231 we can reasonably infer that a few scattered and anomalously high  $\delta^{13}\text{C}_{\text{org}}$  values from microfacies

Formatted: Font color: Blue

Formatted: Subscript

Formatted: Font color: Custom  
Color(RGB(0,128,172))

232 1, 3 and 4 in the Wölong section may also be influenced by compositional mixing (Fig. 4).

### 233 5.2. The T-OAE record in the Tibetan Himalaya

234 As noted earlier, the overall  $\delta^{13}\text{C}_{\text{org}}$  trend in the Nianduo section is comparable to that  
235 recognized from well-preserved T-OAE of siliciclastic and carbonate successions elsewhere (e.g.,  
236 Kemp et al., 2005; Hesselbo et al., 2007; Hermoso et al., 2009, 2012; Trecalli et al., 2012;  
237 Sabatino et al., 2013; Figs. 6 and 7). The Tethyan Himalaya was a mature and tectonically  
238 quiescent passive margin of northern India, with smooth subsidence during the Jurassic  
239 (Sciunnach and Garzanti, 2012). Therefore, our studied Tibetan Himalayan sections can be readily  
240 correlated with each other on the basis of the characteristic top *Lithiotis* beds and associated  
241 flooding surfaces (Fig. 4). This correlation indicates that the onset of the  $\delta^{13}\text{C}_{\text{org}}$  excursion of the  
242 Nianduo section is marked by environmental and biotic changes, i.e., a sharp facies change,  
243 benthic extinction level, development of dysoxic bottom waters (Wignall et al., 2006; Han et al.,  
244 2016) and TOC increase (Fig. 3 and 4). As noted in section 2.2, we attribute these marked changes  
245 to the onset of the T-OAE owing to the biostratigraphic age constraints in the sections, and  
246 because the onset of our new  $\delta^{13}\text{C}_{\text{org}}$  excursion agrees well with the suggested correlation between  
247 the abrupt positive  $\delta^{34}\text{S}$  excursion of the Yunjia section and the  $\delta^{34}\text{S}$  excursion recorded across the  
248 T-OAE in Yorkshire, UK (Newton et al. 2011). Indeed, no other excursion in  $\delta^{34}\text{S}$  of this  
249 magnitude is recognized elsewhere in the Jurassic (Gill et al., 2011). Some debate surrounding the  
250 age assignment of the Himalaya strata exists, however. Notably, the extremely high  $\delta^{34}\text{S}$  values  
251 and anomalously low sulfate oxygen isotope values in the Yunjia section (Newton et al., 2011)  
252 suggest that the carbonate-associated sulfate  $\delta^{34}\text{S}$  ( $\delta^{34}\text{S}_{\text{CAS}}$ ) signal in this section might have been  
253 modified by diagenesis (Gill et al., 2011). However, a recent study shows that  $\delta^{34}\text{S}_{\text{CAS}}$  can



254 withstand burial diagenesis and reliably preserve a record of ambient seawater sulfate and early  
255 diagenetic redox processes (Fichtner et al., 2017). A further consideration is that a second, broad  
256 negative  $\delta^{13}\text{C}$  CIE was reported in the bottom part of the Yunjia section (~2–27 m, shaded interval  
257 on Fig. 4), which was considered as the possible characteristic T-OAE excursion due to both its  
258 shape and the occurrence of rare calcareous nannofossils higher in the section (~88 m) that were  
259 constrained to an early mid-Aalenian age (Fig. 4; Wignall et al., 2006). Given these observations,  
260 the rapid  $\delta^{34}\text{S}$  positive excursion above this  $\delta^{13}\text{C}_{\text{org}}$  negative CIE could be regarded as a possible  
261 Aalenian event (Newton et al., 2011). Further combined with additional anomalously high  $\delta^{13}\text{C}_{\text{org}}$   
262 values ( $> -27\text{‰}$ ) in the Tibetan Himalayan sections, Gill et al. (2011) also thought that the  
263 Tibetan  $\delta^{34}\text{S}$  excursion ~~probably represents~~ could represent a stratigraphically higher event.  
264 However, the onset of this lower CIE in the Yunjia section is not marked by any environmental  
265 and biotic changes, and if this CIE was the T-OAE then the extinction level of the *Lithiotis*  
266 bivalves would be late Toarcian, which is considered unlikely (Newton et al., 2011). In addition,  
267 according to the available biostratigraphy and chemostratigraphy, we note that: 1) the CIE  
268 between ~2 and ~27 m occurs at a position in the *Orbitopsella* foraminifera-rich horizons (Wignall  
269 et al., 2006; Han et al., 2016), which most probably indicates a late Pliensbachian age  
270 (BouDagher-Fadel, 2008); 2) it is hard to reconcile the position of ostensible mid-Aalenian  
271 calcareous nanofossils found at the base of the Nieniexionglä Formation (12 m above the  
272 Pupuga-Nieniexionglä boundary) by Wignall et al. (2006) with the position of middle-late  
273 Toarcian ammonites found in the lower Nieniexionglä Formation by Yin (2010), and 3) as  
274 discussed in section 5.1, the absolute  $\delta^{13}\text{C}_{\text{org}}$  values of the Tibetan sections broadly correspond to  
275 those of the western coeval carbonate platforms. Hence, the biostratigraphic and

276 chemostratigraphic constraints here suggest that the age assignment of the Yunjia section by  
277 [Wignall et al. \(2006\)](#) is incorrect, and the Pupuga–Nieniexiongla transition does indeed  
278 correspond to the onset of the T-OAE.

279 The  $\delta^{13}\text{C}_{\text{org}}$  trend of the Wölong section close to the onset of the T-OAE does not correspond  
280 well to that of the Nianduo section ([Fig. 4](#)). This [difference](#) could be due to [sedimentary](#)  
281 [gaps/hiatuses](#) caused by subaerial exposure in [a](#) shallow platform environment. In addition,  
282 although the  $\delta^{13}\text{C}_{\text{carb}}$  records in the Nianduo section overall show a negative CIE around -1.5‰, its  
283 shape and magnitude are significantly different from those of the typical T-OAE CIE elsewhere  
284 (e.g., [Kemp et al., 2005](#); [Hesselbo et al., 2007](#); [Hermoso et al., 2009](#), [Sabatino et al., 2013](#), [Them](#)  
285 [et al., 2017](#)). Such a phenomenon also occurs in the  $\delta^{13}\text{C}_{\text{carb}}$  expression of the Toarcian CIE in  
286 several Toarcian shallow-water [carbonates](#)[carbonate successions](#) elsewhere ([Woodfine et al., 2008](#);  
287 [Trecalli et al., 2012](#)). Moreover, in other marine settings, many coeval  $\delta^{13}\text{C}_{\text{carb}}$  records in bulk  
288 carbonate and belemnites from western Tethys also do not show obvious negative CIE  
289 shapes/magnitudes that match with CIEs recorded in organic matter (e.g., [Hesselbo et al., 2000](#);  
290 [Jenkyns et al., 2002](#); [van de Schootbrugge et al., 2005](#); [Gill et al., 2011](#)).

### 291 5.3. Intensified storm events and extreme warmth during the early Toarcian

292 A key feature of the Toarcian CIE interval in both the Nianduo and Wölong sections is the  
293 common occurrence of coarse-grained deposits and sedimentary structures associated with  
294 high-energy conditions within the otherwise low-energy carbonate ramp environment of the  
295 Nieniexiongla Formation (see [4.2](#), [Figs. 3 and 4](#)). HCS/SCS and wave rippled surfaces are  
296 important storm-generated sedimentary structures formed under oscillating wave effects  
297 ([Dalrymple and Hoogendoorn, 1997](#)). Gutter casts are generally attributed to powerful

298 unidirectional currents created during the rising and peak phases of storms (Myrow and Southard,  
299 1996). However, recent studies have shown that abundant occurrence of HCS/SCS within  
300 sandstone beds that infilled gutter casts indicates that gutter erosion and rapid subsequent infill can  
301 be ascribed to offshore-directed and oscillatory-dominant combined flows during storms (e.g.,  
302 Collins et al., 2017). Therefore, the high-frequency gutter casts, HCS/SCS, and ripple marks in the  
303 studied sections clearly indicate the process of storms. Other abundant structures occurring in  
304 coarse-grained beds, like parallel laminations, climbing ripples, graded bedding and sharp erosive  
305 bases, are similar to those of turbidites formed under traction currents. However, these units  
306 cannot be clearly identified as turbidites in the Nianduo and Wölong sections because  
307 characteristic structures formed under unidirectional flow (flute casts and current ripples), as well  
308 as Bouma-style grading, were not observed.

309 Storm-related beds in the Nianduo and Wölong sections are abundant within the T-OAE  
310 interval, after maximum flooding at the Pupuga–Nieniexiongla boundary. Two earlier marine  
311 transgressions are recorded in Pliensbachian strata of the Pupuga Formation (Han et al., 2016), but  
312 storm deposits were not observed within these older transgressive sequences. This observation  
313 indicates that increased storm bed deposition/activity was independent of changes in sea level, but  
314 closely linked to the T-OAE. Similarly, geochemical and sedimentological data have emerged in  
315 recent years to indicate that many other tropical/subtropical zones over a latitudinal range of 18°N  
316 to 35°N in the northern hemisphere of the western Tethys were also influenced by frequent storm  
317 events within the T-OAE, as summarized by Krencker et al. (2015). These storm deposits are  
318 present in siliciclastic- and carbonate-dominated settings along the western Tethys, especially in  
319 deeper outer carbonate ramp and (hemi)pelagic environments (e.g., Suan et al., 2013; Pittet et al.,

320 2014; Krencker et al., 2015; Han et al., 2016). Recent work by Izumi et al. (2018) has also  
321 demonstrated evidence of storm activity within the T-OAE in the shallow water margin of western  
322 Panthalassa. Thus, an enhanced intensity of storm events during the early Toarcian can be inferred  
323 that resulted in a basinward shift and deepening of effective storm wave base.

324 Two primary mechanisms can lead to deposition of storm beds: (1) winter storms and (2)  
325 tropical cyclones (Masselink and van Heteren, 2014). The common occurrence of storm-generated  
326 deposits in low latitudes (18–35°, Fig. 8) during the T-OAE excludes winter storms as the  
327 predominant phenomenon, because these are generated by disturbances at the boundary between  
328 warm tropical and cold polar air masses confined to mid- to high-latitudes (30–60°) (Masselink  
329 and van Heteren, 2014). By contrast, tropical cyclones are usually generated at low latitudes on  
330 both sides of the Equator by enthalpy flux from condensation of rising warm and moist air, which  
331 is essentially tied to elevated sea-surface temperature (>26.5 °C; Gray, 1968). Evidence from  $\delta^{18}\text{O}$   
332 data from brachiopods, belemnites and fish teeth from the western Tethys suggest that seawater  
333 temperature rose significantly across the T-OAE interval (4–7 °C, e.g., Gómez et al., 2008; Suan et  
334 al., 2010; Dera et al., 2011). These results support a cause-and-effect relationship between extreme  
335 warmth and increased tropical cyclones that resulted in widely distributed storm deposits along the  
336 western Tethyan margins, as suggested by Krencker et al. (2015). Recent climate models further  
337 confirm that elevated  $\text{CO}_2$  concentration and sea-surface temperature can trigger more frequent  
338 and intense tropical cyclones, and also lead to a poleward expansion of storms (Emanuel, 2016;  
339 Korty et al., 2017).

340 5.4 Possible mechanisms for biotic carbonate-platform demise and delayed recovery during the  
341 early Toarcian

342 The correlation between the Tethyan carbonate-platform successions indicates that the top  
343 *Lithiotis* horizon in each section coincides with abrupt facies changes coincident with the onset of  
344 the  $\delta^{13}\text{C}$  CIE and biotic platform demise by drowning or switching to ~~chemical-type~~non-skeletal  
345 carbonates (Fig. 7; Treccalli et al., 2012; Sabatino et al., 2013). Based on the chemostratigraphy  
346 and biostratigraphy, the late Pliensbachian–earliest Toarcian Kioto platform was a healthy  
347 carbonate platform dominated by hyper-productive massive mound-building bivalves (*Lithiotis*  
348 group), just like other tropical Tethyan and Panthalassan shallow-water carbonate platforms during  
349 the Early Jurassic (Fraser et al., 2004; Franceschi et al., 2014). The drowning of these platforms in  
350 the early Toarcian during the T-OAE was a regional, if not global, phenomenon. Notably, in the  
351 western Tethys (Fig. 8), the Pliensbachian–earliest Toarcian *Lithiotis* limestones of the NW  
352 Adriatic carbonate platform (Slovenia, central and western Croatia and western Bosnia) were  
353 directly overlain by early Toarcian dark spotted limestones (Vlahović et al., 2005; Sabatino et al.,  
354 2013), and deposits with abundant *Lithiotis* bivalves, sponge, and coral of the Djebel Bou Dahar  
355 platform were covered by Toarcian silty shale and limestones/marl alternations (Merino-Tomé et  
356 al., 2012). However, some platforms experienced transient drowning or shifted to ~~a-chemical~~an  
357 unfossiliferous platform type. The shallow-water carbonates rich in *Lithiotis* bivalves of the  
358 western Trento and Campania–Lucania platforms turned to clay-rich facies, and were locally  
359 replaced by crinoid-rich and unfossiliferous oolitic sediments, respectively (Woodfine et al., 2008).  
360 Several resilient platforms (Apennine and Pelagonian platforms, and the rest of NW Adriatic  
361 platform) changed from biotic platform type, dominated by *Lithiotis/P. mediterraneus*, to

362 unfossiliferous ~~chemical~~ oolitic platform (Vlahović et al., 2005; Scherreiks et al., 2010; Trecalli et  
363 al., 2012). These observations show that the demise of early Toarcian biotic platforms through  
364 either drowning or changing to fossil-scarce oolitic platforms was prevalent along the entire  
365 Tethyan tropical/subtropical realms (Fig. 8).

366 Some areas of the western Tethys were located in a relatively tectonically active area during  
367 the early Toarcian, and hence tectonic subsidence could be the major factor that led to drowning of  
368 some platforms (Lachkar et al., 2009; Merino-Tomé et al., 2012). However, this process alone was  
369 unlikely to have been a significant causal influence on Kioto platform drowning in the Tethyan  
370 Himalaya because the mature passive margin of northern India was relatively tectonically  
371 quiescent, with smooth reconstructed subsidence curves through the early Jurassic (Sciunnach and  
372 Garzanti, 2012). Several meters of sea-level rise occurred during the early Toarcian at the  
373 *tenuicostatum (antiquum)–falciferum* zone transition (Suan et al., 2010, 2011). Nevertheless, for a  
374 healthy and highly productive platform, carbonate production should have been fast enough to  
375 keep up with this rise (Schlager, 1981; Godet, 2013).

376 A number of key palaeoenvironmental factors, such as nutrient excesses, anoxic/suboxic  
377 conditions, acidification, clastic delivery, elevated temperature, or a combination of these, have  
378 been suggested as potential triggering mechanisms for drowning of carbonate platforms in the  
379 geological record (Godet, 2013). Importantly, within the resolution of the  $\delta^{13}\text{C}$  data, the extensive  
380 biotic platform drowning or shifting to fossil-scarce oolitic platform occurs across the first phase  
381 of the T-OAE CIE, i.e., just before minimum isotopic values are reached (Fig. 7). The  
382 environmental deterioration of the global ocean associated with the likely large-scale release of  
383 carbon into the ocean-atmosphere system most probably led to extensive biotic platform demise.

384 The T-OAE was associated with increased continental discharge and nutrient input (Cohen et al.,  
385 2004; Jenkyns, 2010; Brazier et al., 2015; Izumi et al., 2018). However, deeper marine shales and  
386 siltstones representing clastic input and phosphatic hardgrounds reflecting eutrophic conditions are  
387 not observed on the top of the drowning unconformity on the eastern Tethyan Kioto platform.  
388 According to detailed microfacies analysis by Han et al. (2016) and our Ti data (Fig. 3), the  
389 shallow-marine carbonates are mainly overlain by lime mudstones (0–6 m) and the level of the  
390 first clastic-rich unit occurs 0.4 m above the drowning boundary. These facts indicate that there  
391 was no immediate increase in clastic delivery and nutrient input when the Kioto platform drowned.  
392 The proxies mentioned above reflecting increased clastic and nutrient input were also not reported  
393 at the boundary of the facies change in the western Tethyan Apennine and Adriatic platforms in  
394 the early Toarcian (Trecalli et al., 2012; Sabatino et al., 2013). Therefore, enhanced clastic input  
395 and subsequent eutrophication are unlikely to explain the entire Tethyan platform demise in the  
396 early Toarcian. Oxygen-depleted conditions likely influenced numerous Tethyan continental  
397 margins, because box-modeling of sulfur isotope changes suggest that pyrite burial in the NW  
398 Tethys alone could not explain the positive  $\delta^{34}\text{S}$  excursion (Gill et al., 2011). However, the mean  
399 framboid diameter distribution (5.96–8.35  $\mu\text{m}$ ) on the Kioto platform (Wignall et al., 2006) and  
400 the manganese chemostratigraphy on the Adriatic carbonate platform (Sabatino et al., 2013)  
401 suggests a sudden change from oxygen-rich to relatively lower dissolved oxygen contents in the  
402 bottom waters, which could have played a role in the abrupt demise of the Tethyan carbonate  
403 platforms. Ocean acidification also has been invoked to explain the demise of biotic platforms at  
404 the onset of the T-OAE because the prolific *Lithotia/P. mediterraneus* are expected to be  
405 vulnerable to a reduction of carbonate saturation caused by a dramatic decrease of pH (Trecalli et

406 al., 2012). This hypothesis seems to be reasonable on the basis of the estimated mass and rate of  
407 carbon release during the T-OAE (McElwain et al., 2005). As discussed above, extreme warmth  
408 likely prevailed along the entire tropical/subtropical Tethys through the T-OAE. Recent studies  
409 further show that a significant increase in seawater temperature, around the  
410 *tenuicostatum-falciferum* zone boundary of early Toarcian age, marks the mass extinction level  
411 (Gómez et al., 2008; Gómez and Goy, 2011). Thus, warming that possibly combined with oceanic  
412 acidification and slight oxygen depletion, likely led to mass extinction of benthic fauna and biotic  
413 carbonate-platform drowning/changing to a ~~chemical~~non-skeletal platform.

414 As mentioned above, after the early Toarcian biocalcification crisis, several resilient  
415 platforms of the western Tethys quickly changed from biotic platforms, dominated by *Lithiotis/P.*  
416 *mediterraneus*, to unfossiliferous ~~chemical~~ oolitic platforms, probably due to the rapid rebound of  
417 carbonate supersaturation in shallow marine environments (Vlahović et al., 2005; Scherreiks et al.,  
418 2010; Trecalli et al., 2012). If other conditions were favourable, the rapid recovery of ocean  
419 alkalinity and carbonate saturation should have promoted the thriving of biotic platforms, while  
420 unfossiliferous oolitic platforms developed extensively. Consequently, after the T-OAE biotic  
421 crisis, extreme warmth seems to have been the major factor that suppressed and postponed the  
422 recovery of biotic platforms dominated by reef-building corals or bivalves. Such a rapid and  
423 persistent warming could have triggered a severe biotic crisis, and was contemporaneously  
424 beneficial to calcium carbonate precipitation, which further facilitated the wide distribution of  
425 ~~chemical~~non-skeletal platforms in shallow settings with carbonate-supersaturated seawater.  
426 Therefore, extreme and persistent warming conditions can reasonably explain the coexistent and  
427 prevalent pattern of biotic platform demise by shifting to unfossiliferous oolitic



428 platforms/drowning in shallow/relative deeper settings with/without carbonate-supersaturated  
429 seawater along the entire Tethys.

## 430 **6. Conclusions**

431 This study reports T-OAE records from a carbonate platform exposed in the Tibetan  
432 Himalaya, and originally deposited on the open SE Tethyan margin of the southern hemisphere.  
433 Based on new biostratigraphical, geochemical and sedimentological data, we have reconstructed  
434 palaeoenvironmental and palaeoclimatic changes of the northern Indian margin through the late  
435 Pliensbachian–early Toarcian interval, encompassing the T-OAE.  $\delta^{13}\text{C}_{\text{org}}$  data from the Nianduo  
436 succession of this platform delineates the T-OAE CIE with a magnitude of  $-2.5\%$ , but a CIE with  
437 a reduced magnitude of  $-1.5\%$  is present in  $\delta^{13}\text{C}_{\text{carb}}$  data. The Wölong succession illustrates only  
438 a recovery trend in  $\delta^{13}\text{C}_{\text{org}}$  data, and not a clear CIE.

439 The common occurrence of storm deposits likely associated with tropical weather systems  
440 indicates that the well-established and marked global warming during the T-OAE severely  
441 influenced the eastern Tethyan margin. This feature of both the Nianduo and Wölong sections is  
442 similar to the observations of storm deposits made in the western Tethys of the northern  
443 hemisphere by [Krencker et al. \(2015\)](#), who also linked such storms to climate warming. The  
444 extreme warm conditions, in response to carbon release during the T-OAE, likely played a key  
445 role in the observed sudden biotic platform demise recorded in our Tibetan sections, and also  
446 observed across the wider tropical/subtropical Tethys. After the onset of the early Toarcian CIE,  
447 ocean alkalinity and carbonate saturation might have quickly recovered from the oceanic  
448 acidification, leading to conditions favorable for the extensive development of  
449 ~~chemical~~non-skeletal platforms in shallow waters ([Trecalli et al., 2012](#)). Nevertheless, the

450 persistence of extreme warm conditions through the early Toarcian could have suppressed and  
451 postponed the redevelopment of biotic platforms dominated by reef-building bivalves and/or  
452 corals.

#### 453 **Acknowledgements**

454 We are grateful to Zhifei Liu for TOC and  $\delta^{13}\text{C}_{\text{carb}}$  analyses at the Tongji University. We thank also  
455 Wei An, Bo Zhou and Shiyi Li for their assistance in the field, and Zhicheng Huang, Yiwei Xu and  
456 Weiwei Xue for their help in the laboratory, and Chao Chang, Tianchen He and Bolin Zhang for  
457 their helpful discussion. Hugh Jenkyns commented on a draft of the manuscript. We would also  
458 like to thank Editor Derek Vance, Christopher Pearce and two anonymous reviewers whose  
459 comments greatly improved the manuscript. This study was financially supported by the National  
460 Natural Science Funds for Distinguished Young Scholar in China (41525007). DBK acknowledges  
461 support of NERC Fellowship NE/I02089X/1. This is a contribution to the IGCP Project 655.

#### 462 **References**

- 463 Al-Suwaidi, A.H., Angelozzi, G.N., Baudin, F., Damborenea, S.E., Hesselbo, S.P., Jenkyns, H.C.,  
464 Mancenido, M.O., Riccardi, A.C., 2010. First record of the Early Toarcian Oceanic  
465 Anoxic Event from the Southern Hemisphere, Neuquen Basin, Argentina. *J. Geol. Soc.*  
466 *Lond.* 167, 633-636.
- 467 Al-Suwaidi, A.H., Hesselbo, S.P., Damborenea, S.E., Mancenido, M.O., Jenkyns, H.C., Riccardi,  
468 A.C., Angelozzi, G.N., Baudin, F., 2016. The Toarcian Oceanic Anoxic Event (Early  
469 Jurassic) in the Neuquen Basin, Argentina: A Reassessment of Age and Carbon Isotope  
470 Stratigraphy. *J. Geol.* 124, 171-193.
- 471 Bodin, S., Krencker, F.N., Kothe, T., Hoffmann, R., Mattioli, E., Heimhofer, U., Kabiri, L., 2016.

472 Perturbation of the carbon cycle during the late Pliensbachian - early Toarcian: New  
473 insight from high-resolution carbon isotope records in Morocco. *J. Afr. Earth. Sci.* 116,  
474 89-104.

475 BouDagher-Fadel, M.K., 2008. Evolution and geological significance of larger benthic  
476 foraminifera. Elsevier, Amsterdam., vol. 404, pp. 1-544.

477 Brasier, M., 1990. The carbon and oxygen isotope record of the Precambrian-Cambrian boundary  
478 interval in China and Iran and their correlation. *Geol. Mag.* 127, 319-332.

479 Brazier, J.M., Suan, G., Tacail, T., Simon, L., Martin, J.E., Mattioli, E., Baiter, V., 2015. Calcium  
480 isotope evidence for dramatic increase of continental weathering during the Toarcian  
481 oceanic anoxic event (Early Jurassic). *Earth Planet. Sci. Lett.* 411, 164-176.

482 Caruthers, A.H., Grocke, D.R., Smith, P.L., 2011. The significance of an Early Jurassic (Toarcian)  
483 carbon-isotope excursion in Haida Gwaii (Queen Charlotte Islands), British Columbia,  
484 Canada. *Earth Planet. Sci. Lett.* 307, 19-26.

485 Cohen, A.S., Coe, A.L., Harding, S.M., Schwark, L., 2004. Osmium isotope evidence for the  
486 regulation of atmospheric CO<sub>2</sub> by continental weathering. *Geology* 32, 157-160.

487 Collins, D.S., Johnson, H.D., Allison, P.A., Guilpain, P., Damit, A.R., 2017. Coupled 'storm-flood'  
488 depositional model: Application to the Miocene–Modern Baram Delta Province,  
489 north-west Borneo. *Sedimentology* 64, 1203-1235.

490 Dalrymple, R.W., Hoogendoorn, E.L., 1997. Erosion and deposition on migrating  
491 shoreface-attached ridges, Sable island, eastern Canada. *Geoscience Canada* 24, 25-36.

492 Dera, G., Brigaud, B., Monna, F., Laffont, R., Puceat, E., Deconinck, J.F., Pellenard, P.,  
493 Joachimski, M.M., Durlet, C., 2011. Climatic ups and downs in a disturbed Jurassic world.

494 Geology 39, 215-218.

495 Emanuel, K., 2016. Will Global Warming Make Hurricane Forecasting More Difficult? Bull. Am.  
496 Meteorol. Soc., 495-501.

497 Fichtner, V., Strauss, H., Immenhauser, A., Buhl, D., Neuser, R.D., Niedermayr, A., 2017.  
498 Diagenesis of carbonate associated sulfate. Chem. Geol. 463, 61-75.

499 Franceschi, M., Dal Corso, J., Posenato, R., Roghi, G., Masetti, D., Jenkyns, H.C., 2014. Early  
500 Pliensbachian (Early Jurassic) C-isotope perturbation and the diffusion of the Lithiotis  
501 Fauna: insights from the western Tethys. Palaeogeogr. Palaeoclimatol. Palaeoecol. 410,  
502 255-263.

503 Fraser, N.M., Bottjer, D.J., Fischer, A.G., 2004. Dissecting "Lithiotis" bivalves: implications for  
504 the Early Jurassic reef eclipse. Palaios 19, 51-67.

505 Fu, X., Wang, J., Feng, X., Wang, D., Chen, W., Song, C., Zeng, S., 2016. Early Jurassic  
506 carbon-isotope excursion in the Qiangtang Basin (Tibet), the eastern Tethys: Implications  
507 for the Toarcian Oceanic anoxic event. Chem. Geol. 442, 62-72.

508 Gómez, J.J., Goy, A., 2011. Warming-driven mass extinction in the Early Toarcian (Early Jurassic)  
509 of northern and central Spain. Correlation with other time-equivalent European sections.  
510 Palaeogeogr. Palaeoclimatol. Palaeoecol. 306, 176-195.

511 Gómez, J.J., Goy, A., Canales, M.L., 2008. Seawater temperature and carbon isotope variations in  
512 belemnites linked to mass extinction during the Toarcian (Early Jurassic) in Central and  
513 Northern Spain. Comparison with other European sections. Palaeogeogr. Palaeoclimatol.  
514 Palaeoecol. 258, 28-58.

515 Gansser, 1964. Geology of the Himalayas. Interscience Publishers John Wiley and Sons, New

516 York (289 pp.).

517 Gill, B.C., Lyons, T.W., Jenkyns, H.C., 2011. A global perturbation to the sulfur cycle during the  
518 Toarcian Oceanic Anoxic Event. *Earth Planet. Sci. Lett.* 312, 484-496.

519 Godet, A., 2013. Drowning unconformities: Palaeoenvironmental significance and involvement of  
520 global processes. *Sediment. Geol.* 293, 45-66.

521 Golonka, J., 2007. Phanerozoic Palaeoenvironment and Paleolithofacies Maps. *Mesozoic. Geologia*  
522 35, 589-654.

523 Gröcke, D.R., Hori, R.S., Trabucho-Alexandre, J., Kemp, D.B., Schwark, L., 2011. An open ocean  
524 record of the Toarcian oceanic anoxic event. *Solid Earth* 2, 245-257.

525 Gray, W.M., 1968. Global view of the origin of tropical disturbances and storms. *Mon. Weather.*  
526 *Rev.* 96, 669-900.

527 Han, Z., Hu, X.M., Li, J., Garzanti, E., 2016. Jurassic carbonate microfacies and relative sea-level  
528 changes in the Tethys Himalaya (southern Tibet). *Palaeogeogr. Palaeoclimatol. Palaeoecol.*  
529 456, 1-20.

530 Hermoso, M., Le Callonnec, L., Minoletti, F., Renard, M., Hesselbo, S.P., 2009. Expression of the  
531 Early Toarcian negative carbon-isotope excursion in separated carbonate microfractions  
532 (Jurassic, Paris Basin). *Earth Planet. Sci. Lett.* 277, 194-203.

533 Hermoso, M., Minoletti, F., Rickaby, R.E.M., Hesselbo, S.P., Baudin, F., Jenkyns, H.C., 2012.  
534 Dynamics of a stepped carbon-isotope excursion: Ultra high-resolution study of Early  
535 Toarcian environmental change. *Earth Planet. Sci. Lett.* 319, 45-54.

536 Hesselbo, S.P., Grocke, D.R., Jenkyns, H.C., Bjerrum, C.J., Farrimond, P., Morgans Bell, H.S.,  
537 2000. Massive dissociation of gas hydrate during a Jurassic oceanic anoxic event. *Nature*

538 406, 392-395.

539 Hesselbo, S.P., Jenkyns, H.C., Duarte, L.V., Oliveira, L.C.V., 2007. Carbon-isotope record of the  
540 Early Jurassic (Toarcian) Oceanic Anoxic Event from fossil wood and marine carbonate  
541 (Lusitanian Basin, Portugal). *Earth Planet. Sci. Lett.* 253, 455-470.

542 Hesselbo, S.P., Pieńkowski, G., 2011. Stepwise atmospheric carbon-isotope excursion during the  
543 Toarcian Oceanic Anoxic Event (Early Jurassic, Polish Basin). *Earth Planet. Sci. Lett.* 301,  
544 365-372.

545 Huang, W.T., van Hinsbergen, D.J., Dekkers, M.J., Garzanti, E., Dupont - Nivet, G., Lippert, P.C.,  
546 Li, X.C., Maffione, M., Langereis, C.G., Hu, X.M., 2015. Paleolatitudes of the Tibetan  
547 Himalaya from primary and secondary magnetizations of Jurassic to Lower Cretaceous  
548 sedimentary rocks. *Geochem. Geophys. Geosyst.* 16, 77-100.

549 Izumi, K., Kemp, D.B., Itamiya, S., Inui, M., 2018. Sedimentary evidence for enhanced  
550 hydrological cycling in response to rapid carbon release during the early Toarcian oceanic  
551 anoxic event. *Earth Planet. Sci. Lett.* 481, 162-170.

552 Jadoul, F., Berra, F., Garzanti, E., 1998. The Tethys Himalayan passive margin from Late Triassic  
553 to Early Cretaceous (South Tibet). *J. Asian. Earth. Sci.* 16, 173-194.

554 Jenkyns, H.C., 1988. The early Toarcian (Jurassic) anoxic event; stratigraphic, sedimentary and  
555 geochemical evidence. *Am. J. Sci.* 288, 101-151.

556 Jenkyns, H.C., 2010. Geochemistry of oceanic anoxic events. *Geochem. Geophys. Geosyst.* 11,  
557 1-30.

558 Jenkyns, H.C., Jones, C.E., Grocke, D.R., Hesselbo, S.P., Parkinson, D.N., 2002.  
559 Chemostratigraphy of the Jurassic System: applications, limitations and implications for

560 palaeoceanography. *J. Geol. Soc. Lond.* 159, 351-378.

561 Kaufman, A.J., Knoll, A.H., 1995. Neoproterozoic variations in the C-isotopic composition of  
562 seawater: stratigraphic and biogeochemical implications. *Precambrian Res.* 73, 27-49.

563 Kemp, D.B., Coe, A.L., Cohen, A.S., Schwark, L., 2005. Astronomical pacing of methane release  
564 in the Early Jurassic period. *Nature* 437, 396-399.

565 Kemp, D.B., Izumi, K., 2014. Multiproxy geochemical analysis of a Panthalassic margin record of  
566 the early Toarcian oceanic anoxic event (Toyora area, Japan). *Palaeogeogr. Palaeoclimatol.*  
567 *Palaeoecol.* 414, 332-341.

568 Knoll, A.H., Hayes, J.M., Kaufman, A.J., Swett, K., Lambert, I.B., 1986. Secular variation in  
569 carbon isotope ratios from Upper Proterozoic successions of Svalbard and East Greenland.  
570 *Nature* 321, 832-838.

571 Korty, R.L., Emanuel, K.A., Huber, M., Zamora, R.A., 2017. Tropical Cyclones Downscaled from  
572 Simulations with Very High Carbon Dioxide Levels. *J. Climate.* 30, 649-667.

573 Krencker, F.N., Bodin, S., Suan, G., Heimhofer, U., Kabiri, L., Immenhauser, A., 2015. Toarcian  
574 extreme warmth led to tropical cyclone intensification. *Earth Planet. Sci. Lett.* 425,  
575 120-130.

576 Lachkar, N., Guiraud, M., El Harfi, A., Dommergues, J.L., Dera, G., Durlet, C., 2009. Early  
577 Jurassic normal faulting in a carbonate extensional basin: characterization of tectonically  
578 driven platform drowning (High Atlas rift, Morocco). *J. Geol. Soc. Lond.* 166, 413-430.

579 Littler, K., Hesselbo, S.P., Jenkyns, H.C., 2010. A carbon-isotope perturbation at the  
580 Pliensbachian-Toarcian boundary: evidence from the Lias Group, NE England. *Geol. Mag.*  
581 147, 181-192.

582 Liu, G.H., Einsele, G., 1994. Sedimentary history of the Tethyan basin in the Tibetan Himalayas.  
583 Geol. Rundsch. 83, 32-61.

584 Masselink, G., van Heteren, S., 2014. Response of wave-dominated and mixed-energy barriers to  
585 storms. Mar. Geol. 352, 321-347.

586 McElwain, J.C., Wade-Murphy, J., Hesselbo, S.P., 2005. Changes in carbon dioxide during an  
587 oceanic anoxic event linked to intrusion into Gondwana coals. Nature 435, 479-482.

588 Merino-Tomé, O., Della Porta, G., Kenter, J.A.M., Verwer, K., Harris, P., Adams, E.W., Playton, T.,  
589 Corrochano, D., 2012. Sequence development in an isolated carbonate platform (Lower  
590 Jurassic, Djebel Bou Dahar, High Atlas, Morocco): influence of tectonics, eustacy and  
591 carbonate production. Sedimentology 59, 118-155.

592 Myrow, P.M., Southard, J.B., 1996. Tempestite deposition. J. Sediment. Res. 66, 875-887.

593 Newton, R.J., Reeves, E.P., Kafousia, N., Wignall, P.B., Bottrell, S.H., Sha, J.-G., 2011. Low  
594 marine sulfate concentrations and the isolation of the European epicontinental sea during  
595 the Early Jurassic. Geology 39, 7-10.

596 Oehlert, A.M., Swart, P.K., 2014. Interpreting carbonate and organic carbon isotope covariance in  
597 the sedimentary record. Nat. Commun. 5, 4672.

598 Pearce, C.R., Cohen, A.S., Coe, A.L., Burton, K.W., 2008. Molybdenum isotope evidence for  
599 global ocean anoxia coupled with perturbations to the carbon cycle during the Early  
600 Jurassic. Geology 36, 231-234.

601 Pittet, B., Suan, G., Lenoir, F., Duarte, L.V., Mattioli, E., 2014. Carbon isotope evidence for  
602 sedimentary discontinuities in the lower Toarcian of the Lusitanian Basin (Portugal): Sea  
603 level change at the onset of the Oceanic Anoxic Event. Sediment. Geol. 303, 1-14.



604 Sabatino, N., Vlahovic, I., Jenkyns, H.C., Scopelliti, G., Neri, R., Prtoljan, B., Velic, I., 2013.  
605 Carbon-isotope record and palaeoenvironmental changes during the early Toarcian  
606 oceanic anoxic event in shallow-marine carbonates of the Adriatic Carbonate Platform in  
607 Croatia. *Geol. Mag.* 150, 1085-1102.

608 Scherreiks, R., Bosence, D., BouDagher-Fadel, M., Meléndez, G., Baumgartner, P.O., 2010.  
609 Evolution of the Pelagonian carbonate platform complex and the adjacent oceanic realm  
610 in response to plate tectonic forcing (Late Triassic and Jurassic), Evvoia, Greece. *Int. J.*  
611 *Earth Sci. (Geol. Rundsch.)* 99, 1317-1334.

612 Schlager, W., 1981. The paradox of drowned reefs and carbonate platforms. *Geol. Soc. Am. Bull.*  
613 92, 197-211.

614 Sciunnach, D., Garzanti, E., 2012. Subsidence history of the Tethys Himalaya. *Earth-Sci. Rev.* 111,  
615 179-198.

616 Suan, G., Mattioli, E., Pittet, B., Lecuyer, C., Sucheras-Marx, B., Duarte, L.V., Philippe, M.,  
617 Reggiani, L., Martineau, F., 2010. Secular environmental precursors to Early Toarcian  
618 (Jurassic) extreme climate changes. *Earth Planet. Sci. Lett.* 290, 448-458.

619 Suan, G., Nikitenko, B.L., Rogov, M.A., Baudin, F., Spangenberg, J.E., Knyazev, V.G., Glinskikh,  
620 L.A., Goryacheva, A.A., Adatte, T., Riding, J.B., Follmi, K.B., Pittet, B., Mattioli, E.,  
621 Lecuyer, C., 2011. Polar record of Early Jurassic massive carbon injection. *Earth Planet.*  
622 *Sci. Lett.* 312, 102-113.

623 Suan, G., Rulleau, L., Mattioli, E., Sucheras-Marx, B., Rousselle, B., Pittet, B., Vincent, P., Martin,  
624 J.E., Lena, A., Spangenberg, J.E., Follmi, K.B., 2013. Palaeoenvironmental significance  
625 of Toarcian black shales and event deposits from southern Beaujolais, France. *Geol. Mag.*

626 150, 728-742.

627 Suan, G., van de Schootbrugge, B., Adatte, T., Fiebig, J., Oschmann, W., 2015. Calibrating the  
628 magnitude of the Toarcian carbon cycle perturbation. *Paleoceanography* 30, 495-509.

629 Them, T., Gill, B., Caruthers, A., Gröcke, D., Tulskey, E., Martindale, R., Poulton, T., Smith, P.,  
630 2017. High-resolution carbon isotope records of the Toarcian Oceanic Anoxic Event  
631 (Early Jurassic) from North America and implications for the global drivers of the  
632 Toarcian carbon cycle. *Earth Planet. Sci. Lett.* 459, 118-126.

633 Trecalli, A., Spangenberg, J., Adatte, T., Follmi, K.B., Parente, M., 2012. Carbonate platform  
634 evidence of ocean acidification at the onset of the early Toarcian oceanic anoxic event.  
635 *Earth Planet. Sci. Lett.* 357, 214-225.

636 van de Schootbrugge, B., McArthur, J.M., Bailey, T.R., Rosenthal, Y., Wright, J.D., Miller, K.G.,  
637 2005. Toarcian oceanic anoxic event: An assessment of global causes using belemnite C  
638 isotope records. *Paleoceanography* 20, PA3008.

639 Vlahović, I., Tisljar, J., I, Maticec, D., 2005. Evolution of the Adriatic Carbonate Platform:  
640 Palaeogeography, main events and depositional dynamics. *Palaeogeogr. Palaeoclimatol.*  
641 *Palaeoecol.* 220, 333-360.

642 Wignall, P.B., Hallam, A., Newton, R.J., Sha, J.G., Reeves, E., Mattioli, E., Crowley, S., 2006. An  
643 eastern Tethyan (Tibetan) record of the Early Jurassic (Toarcian) mass extinction event.  
644 *Geobiology* 4, 179-190.

645 Woodfine, R.G., Jenkyns, H.C., Sarti, M., Baroncini, F., Violante, C., 2008. The response of two  
646 Tethyan carbonate platforms to the early Toarcian (Jurassic) oceanic anoxic event:  
647 environmental change and differential subsidence. *Sedimentology* 55, 1011-1028.

648 Xu, W., Ruhl, M., Jenkyns, H., Hesselbo, S., Riding, J., Selby, D., Naafs, B., Weijers, J., Pancost,  
649 R., Tegelaar, E., 2017. Carbon sequestration in an expanding lake system during the  
650 Toarcian Oceanic Anoxic Event. *Nat. Geosci.* 10, 129-135.  
651 Yin, J.R., 2010. Jurassic Ammonites of Tibet. Geological Publishing House, Beijing (247 pp.) (in  
652 Chinese with English abstract).

653 **Figure caption**

654 **Fig. 1.** (A) Simplified tectonic map of the Tibetan Plateau showing the major blocks and sutures.  
655 MFT: Main Frontal Thrust; MBT: Main Boundary Thrust; MCT: Main Central Thrust; STDS:  
656 Southern Tibetan Detachment System; ATF: Alty Tagh Fault; KF: Karakorum Fault. (B)  
657 Geological sketch map of the Himalayas showing the studied areas, modified after [Gansser \(1964\)](#).  
658 (C) Road map showing detailed location of three Toarcian sections: Wölong, Nianduo and Yunjia.  
659 (D) Global palaeogeographic setting during the Toarcian showing the northern Indian continental  
660 margin (adapted from [Ron Blakey, <http://jan.ucc.nau.edu/~rcb7/>](#)).

661 **Fig. 2.** Field photographs of the studied sections and storm deposits within the T-OAE interval. (A  
662 and B) Nianduo section and (C and D) Wölong section showing the detailed abrupt facies change  
663 at the Pupuga–Nieniexiongla boundary (dashed white line) within the Pliensbachian–Toarcian  
664 carbonate successions. (E) Ripple marks. (F) Storm beds with HCS/SCS. (G) Sandy beds within  
665 mudstones showing weak HCS. (H) V-shaped gutter casts filled with mixed coarse carbonate and  
666 terrestrial grains showing HCS/SCS.

667 **Fig. 3.** Nianduo section shows stratigraphic distribution of organic carbon isotopes ( $\delta^{13}\text{C}_{\text{org}}$ ),  
668 carbonate carbon and oxygen isotopes ( $\delta^{13}\text{C}_{\text{carb}}$  and  $\delta^{18}\text{O}_{\text{carb}}$ ), total organic carbon (TOC), and Ti.  
669 The  $\delta^{13}\text{C}_{\text{org}}$  data are plotted as different colours based on the facies observed in thin sections of the

670 analysed samples (microfacies 1-4 as shown in legend). Microfacies are: 1 (red datapoints):  
 671 Oolitic grainstone; 2 (black datapoints): Fine-grained peloidal packstone; 3 (green datapoints):  
 672 Sandy peloidal packstone/grainstone; 4 (orange datapoints): Mudstone. The red line through the  
 673 data is the 3-point moving average. Note that this averaging omits the 6 datapoints (circled with  
 674 blue dashed ellipse) at ~10 m height that lie well away from the rest of the data and are likely  
 675 influenced by terrestrial input (see main text for details). Note the distribution of storm beds and  
 676 relative abundance of storm beds within the CIE interval between ~0 and ~10 m.

677 **Fig. 4.** Correlation between the Tibetan sections based on the position of the top *Lithiotis* horizon  
 678 and the Pupuga–Nienixiongla boundary, i.e., the Toarcian maximum flooding surface, facies  
 679 change (Han et al., 2016) and extinction level (Wignall et al., 2006), and carbon- and  
 680 sulfur-isotope stratigraphy.  $\delta^{13}\text{C}_{\text{org}}$  datapoint colour coding is based on the microfacies, as in Fig. 3.  
 681 Red line through the  $\delta^{13}\text{C}_{\text{org}}$  data in both the Nianduo and Wölong sections is the 3-point moving  
 682 average. Moving average for Nianduo section as in Fig. 3. For the Wölong section, 9 anomalously  
 683 high  $\delta^{13}\text{C}_{\text{org}}$  values (in blue dashed ellipse) are omitted from the moving average. These are likely  
 684 influenced by terrestrial input (see main text for details). The Yunjia section shows the  
 685 stratigraphic distribution of organic and carbonate carbon-isotope data ( $\delta^{13}\text{C}_{\text{org}}$  and  $\delta^{13}\text{C}_{\text{carb}}$ ), and  
 686 carbonate-associated sulfate (CAS) isotope data ( $\delta^{34}\text{S}_{\text{CAS}}$ ) (data from Newton et al. 2011 and  
 687 Wignall et al. 2006). T-SIE: Early Toarcian sulfur-isotope excursion. Grey shading between ~2 and  
 688 ~27 m in the Yunjia section delineates CIE recognised in Wignall et al. (2006), see main text for  
 689 details.

690 **Fig. 5.** Cross-plots of  $\delta^{13}\text{C}_{\text{carb}}$ - $\delta^{13}\text{C}_{\text{org}}$  (A),  $\delta^{13}\text{C}_{\text{carb}}$ - $\delta^{18}\text{O}_{\text{carb}}$  (B) and  $\delta^{13}\text{C}_{\text{org}}$ -Ti (C)  
 691 within typical microfacies of the Nianduo section. D shows characteristic microfacies 1 to 4: 1

- Formatted: Font color: Auto
- Formatted: Font color: Auto, Not Superscript/ Subscript
- Formatted: Not Superscript/ Subscript
- Formatted: Font color: Black
- Formatted: Font color: Black, Subscript

692 (red datapoints): Oolitic grainstone; 2 (black datapoints): Fine-grained peloidal packstone; 3  
693 (green datapoints): Sandy peloidal packstone/grainstone; 4 (orange datapoints): Mudstone.

694 **Fig. 6.** Chemostratigraphic correlation of the Pliensbachian–Toarcian transition from the Tibetan  
695 sections in this study with sections from Europe (Hawsker Bottoms, UK; [Cohen et al., 2004](#);  
696 [Kemp et al., 2005](#); [Littler et al., 2010](#), and Peniche, Portugal; [Hesselbo et al., 2007](#)). The profiles  
697 have been correlated using the onset and end of the carbon isotope excursions (CIEs). *P. spin* =  
698 *Pleuroceras spinatum*, Pl. = Pliensbachian. Note that the Wölong section does not show a clear  
699 CIE, see main text for details.

700 **Fig. 7.** Chemostratigraphic and lithological correlation of the Nianduo section with sections from  
701 the Adriatic Carbonate Platform in Croatia ([Sabatino et al., 2013](#)) and the Apennine Carbonate  
702 Platform in southern Italy ([Trecalli et al., 2012](#)). This correlation is based on the boundary of  
703 abrupt facies change from *Lithiotis* limestones to mudstones/oolitic limestones. This change is  
704 broadly consistent with the onset of the Toarcian CIE in each section.

705 **Fig. 8.** (A) Palaeogeographic map of the Tethys Ocean during the Early Jurassic showing the key  
706 locations discussed in the text (modified after [Golonka \(2007\)](#) and [Ron Blakey](#),  
707 <http://jan.ucc.nau.edu/~rcb7/>). The geographic distribution of storm deposits is modified after  
708 [Krencker et al. \(2015\)](#). 1-Dutch Graben, Netherlands, 2-Yorkshire, UK, 3-Dotternhausen, SW  
709 Germany, 4-Sancerre core, Paris Basin, France, 5-ANDRA HTM-102 Borehole, NE France,  
710 6-Lafarge quarry, SE France, 7-Causse Basin, Central-South France, 8-Lusitanian basin, Portugal,  
711 9-Dades Valley, Morocco, 10-Bilong Co, southern Qiangtang. TCP-Trento Carbonate Platform,  
712 AdCP-Adriatic Carbonate Platform, PCP-Pelagonian Carbonate Platform, ACP-Apennine  
713 Carbonate Platform, CLCP-Campania–Lucania Carbonate Platform, DBCP-Djebel Bou Dahar

714 Carbonate Platform, KCP-Kioto Carbonate Platform.

## Highlights

- The T-OAE is recognised on the shallow carbonate platform in southern hemisphere.
- Increased storm deposits point to climatic disturbance related to warming.
- Warmth likely led to the sudden biotic platform demise and delayed their redevelopment.

1 **Carbonate-platform response to the Toarcian Oceanic Anoxic Event in the southern**  
2 **hemisphere: Implications for climatic change and biotic platform demise**

3

4 **Zhong Han**<sup>1</sup>, **Xiumian Hu**<sup>1,\*</sup>, **David B. Kemp**<sup>2</sup>, **Juan Li**<sup>1</sup>

5

*1 State Key Laboratory of Mineral Deposit Research, School of Earth Sciences and Engineering,  
Nanjing University, Nanjing 210023, China*

*2 School of Geosciences, University of Aberdeen, Old Aberdeen AB24 3UE, U.K*

*\*Corresponding author: Dr. Xiumian Hu*

*E-mail: huxm@nju.edu.cn; Tel: 0086 25 89683002*

6 **Abstract**

7 The Toarcian Oceanic Anoxic Event (T-OAE, ~183 Ma) was a profound short-term  
8 environmental perturbation associated with the large-scale release of <sup>13</sup>C-depleted carbon into the  
9 global ocean-atmosphere system, which resulted in a significant negative carbon-isotope  
10 excursion (CIE). The general lack of characteristic T-OAE records outside of the northern  
11 hemisphere means that the precise environmental effects and significance of this event are  
12 uncertain. Many biotic carbonate platforms of the northern hemisphere western Tethys drowned or  
13 shifted to non-skeletal platforms during the early Toarcian. However, southern hemisphere records  
14 of Toarcian carbonate platforms are rare, and thus the extent and significance of biotic platform  
15 demise during the T-OAE is unclear. Here we present high-resolution geochemical and



16 sedimentological data across two Pliensbachian–Toarcian shallow-water carbonate-platform  
17 sections exposed in the Tibetan Himalaya. These sections were located paleogeographically on the  
18 open southeastern tropical Tethyan margin in the southern hemisphere. The T-OAE in the Tibetan  
19 Himalaya is marked by a negative CIE in organic matter. Our sedimentological analysis of the two  
20 sections reveals an abundance of storm deposits within the T-OAE interval, which emphasizes a  
21 close link between warming and tropical storms during the T-OAE event, in line with evidence  
22 recently provided from western Tethyan sections of the northern hemisphere. In addition, our  
23 analysis also reveals extensive biotic carbonate-platform demise by drowning or changing to  
24 non-skeletal carbonates coincident with the onset of the CIE. Taken together, our results suggest  
25 that rapid and pervasive seawater warming in response to carbon release likely played a significant  
26 role in sudden biotic carbonate platform demise, and suppression/postponement of biotic platform  
27 re-development along the whole tropical/subtropical Tethyan margin.

28 **Keywords:** Toarcian Oceanic Anoxic Event; Tibetan Himalaya; Carbon isotopes; Storm deposits;  
29 Carbonate platform; Southern hemisphere.

## 30 **1. Introduction**

31 The early Toarcian Oceanic Anoxic Event (T-OAE, ~183 Ma) was characterized by abrupt  
32 global warming, enhanced weathering rates, expansion of anoxic conditions, and the worldwide  
33 accumulation of organic-rich sediments (e.g., [Jenkyns, 1988, 2010](#); [Cohen et al., 2004](#); [Pearce et](#)  
34 [al., 2008](#); [Dera et al., 2011](#); [Brazier et al., 2015](#); [Fu et al., 2016](#)). It is characteristically marked by  
35 a negative carbon isotope ( $\delta^{13}\text{C}$ ) excursion (CIE) with an amplitude of ~3–8‰, which typically  
36 interrupts a longer-term positive excursion attributable to the global increase in organic carbon  
37 burial. The CIE has been recognised in bulk organic carbon, bulk carbonate, fossil wood and

38 phytoclasts. In some studies, the shift to minimum  $\delta^{13}\text{C}$  values has been shown to occur in discrete,  
39 periodic steps (Kemp et al., 2005; Hesselbo et al., 2007; Hermoso et al., 2009, 2012; Hesselbo and  
40 Pieńkowski, 2011; Them et al., 2017). Two hypotheses have been put forward to explain the CIE:  
41 (i) methane hydrate dissociation from marine sediments and consequent release of  $^{12}\text{C}$  (e.g.,  
42 Hesselbo et al., 2000; Kemp et al., 2005); (ii) thermogenic emission of  $^{12}\text{C}$  induced by the  
43 intrusive emplacement of Karoo-Ferrar sills in organic-rich mudrocks (e.g., McElwain et al.,  
44 2005).

45         Although the T-OAE has been well documented in the western Tethys and Boreal realms (i.e.,  
46 Europe, e.g., Kemp et al., 2005; Hesselbo et al., 2007; Hermoso et al., 2009, 2012), fewer studies  
47 have been conducted elsewhere. Notable exceptions are recent studies from the NE Tethys (Fu et  
48 al., 2016), NW, central and NE Panthalassa (Caruthers et al., 2011; Gröcke et al., 2011; Kemp and  
49 Izumi, 2014), and the Sichuan Lake Basin, China (Xu et al., 2017). In the southern hemisphere,  
50 however, the T-OAE has been reported only from the Neuquén Basin, Argentina, which is a  
51 restricted back-arc rift basin formed during the Mesozoic (Al-Suwaidi et al., 2010, 2016).  
52 Therefore, no record of the T-OAE has been reported from an open-ocean setting in the southern  
53 hemisphere. Consequently, there is uncertainty as to whether the Toarcian CIE and corresponding  
54 environmental perturbations affected the southern hemisphere in the same way as the northern  
55 hemisphere. This has implications for assessing the severity, importance, and casual mechanism(s)  
56 of the event.

57         At the onset of the T-OAE, extensive demise of biotic carbonate platforms occurred in the  
58 western Tethys, attributed variously to the effects of falling carbonate production, tectonics,  
59 eustasy, increased nutrient levels, or oceanic acidification (Woodfine et al., 2008; Lachkar et al.,

60 2009; Merino-Tomé et al., 2012; Trecalli et al., 2012; Sabatino et al., 2013). However, the study of  
61 the relationship between the T-OAE and carbonate-platform evolution has thus far been restricted  
62 to the southern margins of western Tethys at low latitudes of the northern hemisphere.  
63 Consequently, only a localized understanding of carbonate-platform responses to the T-OAE has  
64 hitherto been gained, and the factors that triggered the demise of biotic platforms and delayed their  
65 recovery until well after the event are still uncertain and need to be better constrained.

66 In this paper, we present sedimentological and geochemical data across two uppermost  
67 Pliensbachian to lower Toarcian shallow-marine carbonate platform successions exposed in the  
68 Tibetan Himalaya, deposited at a low latitude (~21.8°S to ~26.1°S) in the southern hemisphere  
69 (Fig. 1A; Huang et al., 2015). We assess the environmental evolution of these platforms through  
70 the T-OAE, and discuss the possible global/regional factors controlling platform evolution and  
71 sedimentology along the Tethyan margin.

## 72 **2. Geological setting**

### 73 *2.1. Tectonic setting*

74 The Tethyan Himalayan Sequence, located between the Indus-Yarlung Zangbo Suture Zone  
75 to the north and the Greater Himalayan Sequence to the south (Fig. 1A and B; Gansser, 1964),  
76 consists mainly of Proterozoic to Eocene carbonate and siliciclastic sedimentary rocks that  
77 originally represented the northern margin deposits of the Indian subcontinent (Fig. 1D; Liu and  
78 Einsele, 1994; Jadoul et al., 1998; Sciunnach and Garzanti, 2012). This unit was traditionally  
79 subdivided into southern and northern zones. The southern zone is dominated by Lower Paleozoic  
80 to Lower Eocene shallow-water carbonates and terrigenous rocks (Liu and Einsele, 1994; Jadoul

81 et al., 1998; Sciunnach and Garzanti, 2012), whereas the northern zone is characterized by  
82 Mesozoic to Paleocene deep-water slope and rise sediments (Liu and Einsele, 1994). During the  
83 Early Jurassic, the Tethyan Himalaya migrated into the southern tropical/subtropical belt, and  
84 carbonate deposits gradually became extensive in the southern zone, forming the Kioto carbonate  
85 platform (Jadoul et al., 1998; Sciunnach and Garzanti, 2012; Huang et al., 2015).

## 86 2.2. Stratigraphy

87 The Nianduo section in the Nyalam area and the Wölong section in the Tingri area are  
88 located in the Tethyan Himalaya on the Kioto carbonate platform (Fig. 1B). Both sections have a  
89 continuously exposed marine sedimentary succession ranging from the upper Lower Jurassic  
90 Pupuga Formation to the lower Middle Jurassic Nieniexiongla Formation (Fig. 2A–D). The  
91 Pupuga Formation represents a shallow-water carbonate platform dominated by  
92 grainstones/packstones deposited under high-energy conditions with occasional influxes of  
93 terrigenous material. The lower-middle Pupuga Formation in both Tingri and Nyalam areas yields  
94 abundant and diversified benthic foraminifera including *Haurania deserta*, *Orbitopsella*  
95 *praecursor*, *Palaeomayncina termieri*, *Amijiella amiji*, *Cyclorbitopsella tibetica*, *Ammobaculites*  
96 *sp.*, *Lituosepta cf. compressa*, *Pseudocyclammina cf. liasica* (Jadoul et al., 1998; Wignall et al.,  
97 2006). These foraminiferal assemblages of the Tibetan Himalaya are similar to those observed in  
98 the Liassic carbonate platforms of the SW Tethyan margin in the northern hemisphere, and  
99 indicate a late Sinemurian–late Pliensbachian age (BouDagher-Fadel, 2008). In the upper Pupuga  
100 Formation, two intervals enriched in *Lithiotis* bivalves respectively occur ~20–30 m and ~3–4 m  
101 below the boundary with the overlying Nieniexiongla Formation in both the Nianduo and Wölong  
102 sections (Figs. 3 and 4). *Lithiotis* bivalves are found in carbonate platforms throughout the tropical

103 Tethys and Panthalassa, where they are limited to strata of late Pliensbachian to early Toarcian age  
104 (Fraser et al., 2004; Franceschi et al., 2014; Bodin et al., 2016). The overlying Nieniexiongla  
105 Formation represents a middle/outer carbonate ramp environment, and is characterized by  
106 mudstones deposited under low-energy conditions intercalated with abundant coarse-grained beds  
107 (Han et al., 2016). In the lower Nieniexiongla Formation, ammonites (*Polyplectus discoides*,  
108 *Dumortieria sp.*, *Phymatoceras cf. crasstcosta*) collected in thin-bedded mudstones near the  
109 Nianduo section were assigned to the *bifrons-levesquei* zones of the middle-late Toarcian (Fig. 3;  
110 Yin, 2010). The upper part of this unit in the Wölong section yields ammonites (*Leptosphinctes*  
111 *sp.*) suggestive of a Bajocian age (Jadoul et al., 1998). In addition to these biostratigraphic  
112 constraints, further important information on the age of the studied stratigraphy can be derived  
113 from available stable sulfur isotope ( $\delta^{34}\text{S}$ ) stratigraphy (Newton et al., 2011). Based on the *lituolid*  
114 foraminifera and *Lithiotis* bivalves, the studied sections can be readily correlated with the nearby  
115 Yunjia section (~500 m away from the Wölong section, Fig. 1C). Newton et al. (2011) suggested  
116 that a marked shift in  $\delta^{34}\text{S}$  data in the Yunjia section close to the Pupuga–Nieniexiongla boundary  
117 can be correlated with a similar shift in the biostratigraphically well-constrained Yorkshire (UK)  
118 section. Based on this correlation, the Pupuga–Nieniexiongla transitional interval is most probably  
119 coeval with the upper *tenuicostatum*-lower *falciferum* ammonite Zone boundary in Europe, and  
120 thus of early Toarcian age.

### 121 3. Material and Methods

122 Rock samples were collected from the Nianduo section (28°40'52"N, 86°08'7"E) of Nyalam  
123 County and the Wölong section (28°29'2"N, 87°02'3"E) of Tingri County in the Tibetan Himalaya  
124 (Fig. 1B and C). Samples were collected with an average spacing of 1 m, reduced to ~0.2–0.3 m in

125 the Nianduo section and 0.1–0.2 m in the Wölong section across the Pupuga–Nieniexiongla  
126 stratigraphic transition.

127 A total of 132 samples from the Nianduo section and 124 samples from the Wölong section  
128 were analyzed for organic carbon-isotope composition ( $\delta^{13}\text{C}_{\text{org}}$ ) at the SINOPEC Wuxi Research  
129 Institute of Petroleum Geology. Powdered samples were treated with 2N HCl at 80°C for at least 3  
130 hours to remove carbonate, and were then washed with distilled water to remove residual HCl.  
131 Organic carbon-isotope analyses were performed on dried samples using a Finnigan MAT 253  
132 mass spectrometer, with an instrumental standard deviation of  $\pm 0.1\%$ . Isotopic measurements  
133 were calibrated to Chinese national standard charcoal sample GBW04407 ( $\delta^{13}\text{C}_{\text{VPDB}} = -22.43\% \pm$   
134  $0.07\%$ ). Results were reported in standard  $\delta$ -notation relative to the Vienna Peedee Belemnite  
135 (VPDB) standard. To supplement our  $\delta^{13}\text{C}_{\text{org}}$  data,  $\delta^{13}\text{C}$  and  $\delta^{18}\text{O}$  of bulk carbonate were measured  
136 on 98 samples across the Pupuga–Nieniexiongla boundary interval in the Nianduo section using a  
137 Finnigan MAT 252 isotope ratio mass spectrometer at the State Key Laboratory of Marine  
138 Geology at Tongji University. The isotope results of  $\delta^{13}\text{C}_{\text{carb}}$  and  $\delta^{18}\text{O}_{\text{carb}}$  were corrected to VPDB  
139 standard, with analytical uncertainties of  $\pm 0.06\%$  and  $\pm 0.08\%$ , respectively.

140 Total organic carbon (TOC) analysis was performed on 69 samples, parallel to the  $\delta^{13}\text{C}_{\text{carb}}$   
141 samples, across the Pupuga–Nieniexiongla boundary interval in the Nianduo section using a Vario  
142 Cube CN elemental analyzer (Elementar, Germany) at the State Key Laboratory of Marine  
143 Geology of Tongji University. Prior to analysis, these samples were treated with 10% HCl for at  
144 least 24 h to remove inorganic carbon. Titanium concentrations was determined on 53 powdered  
145 samples from the Nianduo section using an Olympus Delta Premium handheld XRF (hhXRF)  
146 instrument at the University of Aberdeen. The calibration error (uncertainty) of Ti measurements

147 is better than 0.04%. Reproducibility, based on repeat measurement of a standard, was better than  
148 0.009% (1 s.d., 2.36% relative s.d.).

## 149 **4. Results**

### 150 *4.1. Geochemical data*

#### 151 *4.1.1. Isotope geochemistry*

152 Carbon- and oxygen-isotope data are plotted stratigraphically in Fig. 3 for the Nianduo  
153 section and in Fig. 4 for the Wölong section. In the Nianduo section, a negative CIE of  $\sim -2.5\text{‰}$  is  
154 recorded in organic matter ( $-0.3$  to  $28.4$  m; Fig. 3). This CIE starts at the topmost Pupuga  
155 Formation, just above the top of the *Lithiotis*-rich interval.  $\delta^{13}\text{C}_{\text{org}}$  values are variable between  
156  $-0.3$  m and  $\sim 16$  m during the overall shift to minimum values.  $\delta^{13}\text{C}_{\text{carb}}$  data primarily range  
157 between  $1\text{‰}$  and  $2.5\text{‰}$ , and show an overall negative trend beginning shortly after the  
158 Pupuga–Nieniexionгла boundary ( $\sim 0$  m) and extending to  $\sim 30$  m, with a small magnitude of  
159  $\sim -1.5\text{‰}$ . However,  $\delta^{13}\text{C}_{\text{carb}}$  data do not show the same profile as the  $\delta^{13}\text{C}_{\text{org}}$  data (Fig. 3). The  
160 corresponding oxygen-isotope data mainly range from  $-8$  to  $-5\text{‰}$ , with an average value of  
161  $-6.4\text{‰}$ .

162 Compared to the Nianduo section,  $\delta^{13}\text{C}_{\text{org}}$  data in the Wölong section do not show a  
163 decreasing trend close to the Pupuga–Nieniexionгла boundary (Fig. 4). A broad negative CIE of  
164  $\sim -2.5\text{‰}$  is, however, apparent higher up in the section between  $\sim 8$  m and  $\sim 30$  m. The recovery  
165 profile of this excursion between  $\sim 15$  m and  $\sim 30$  m is similar to the recovery profile of the  $\delta^{13}\text{C}_{\text{org}}$   
166 data between  $\sim 15$  m and  $\sim 30$  m in the Nianduo section.

167 *4.1.2. TOC and elemental content*

168 TOC values from the Nianduo section range from 0.05 to 0.3 wt.%, with an average value of  
169 0.14 wt.% (Fig. 3). An increase in TOC values occurs shortly after the onset of the CIE between  
170 ~0 m and ~8 m. Ti abundance in the Nianduo section is plotted in Fig. 3 and primarily ranges  
171 between 0.05% and 0.15%, with an average value of 0.069%.

172 *4.2. Sedimentological observations*

173 As noted above, and previously by Han et al. (2016), platform-top grainstones deposited  
174 under high-energy conditions of the Pupuga Formation are abruptly overlain by middle/outer ramp  
175 mudstones reflecting low-energy conditions of the Nieniexiongla Formation in the Nianduo and  
176 Wölong sections (0 m datum in both sections). The interval immediately above this flooding  
177 surface in both the Nianduo and Wölong sections is characterized by the common occurrence of  
178 coarse-grained beds, e.g., rudstones, floatstones, siltstones, oolitic grainstones, and peloidal  
179 packstones/wackestones (Han et al., 2016; Figs. 3 and 4). These intervals show abundant and  
180 diverse sedimentary structures such as wave ripples (Fig. 2E) and small-scale hummocky and  
181 swaley cross-stratification (HCS and SCS; Fig. 2F). Some sandy beds within mudstones show  
182 weak HCS individually (Fig. 2G) or just above the U/V-shaped gutter casts (Fig. 2H). In addition,  
183 other sedimentary structures, e.g., parallel laminations, climbing ripples, graded bedding and sharp  
184 erosive bases, are also readily observed both at outcrop and in microfacies (Han et al., 2016).  
185 These coarse-grained beds and related structures are particularly concentrated in the Nianduo  
186 section between ~0 m and ~12 m, coincident with the overall shift to minimum  $\delta^{13}\text{C}_{\text{org}}$  values. In  
187 the Wölong section, they are also concentrated close to the base of the Nieniexiongla Formation.



188 **5. Discussion**

189 *5.1. Diagenetic and source effects on carbon-isotope data*

190 The early Toarcian negative CIE has been widely recorded in a range of marine environments,  
191 including shallow-water carbonate platforms (Kemp et al., 2005, Hesselbo et al., 2007, Woodfine  
192 et al., 2008; Trecalli et al., 2012; Sabatino et al., 2013; Them et al., 2017). However, high-energy  
193 deposits on shallow-water platforms are readily influenced by freshwater diagenesis or organic  
194 matter source changes (Oehlert and Swart, 2014; Suan et al., 2015). The measured  $\delta^{18}\text{O}$  values  
195 ( $>-10\text{‰}$ ) in the Nianduo section, coupled with the absence of any correlation between  $\delta^{18}\text{O}$  and  
196  $\delta^{13}\text{C}_{\text{carb}}$  ( $R^2=0.005$ , Fig. 5A), suggests limited diagenetic influence on the  $\delta^{13}\text{C}_{\text{carb}}$  data (Brasier et  
197 al., 1990; Kaufman and Knoll, 1995). The decoupled  $\delta^{13}\text{C}_{\text{org}}$  and  $\delta^{13}\text{C}_{\text{carb}}$  relationship ( $R^2=0.023$ ,  
198 Fig. 5B) possibly indicates evidence for diagenetic alteration (e.g., Knoll et al., 1986, see also,  
199 however, Oehlert and Swart, 2014). Nevertheless, the overall pattern of  $\delta^{13}\text{C}_{\text{org}}$  changes in the  
200 Nianduo section is comparable to that recognized from well-preserved T-OAE successions  
201 elsewhere (e.g., Kemp et al., 2005; Hesselbo et al., 2007; Hermoso et al., 2009, 2012; Sabatino et  
202 al., 2013, see discussion below), albeit with lower magnitude variations (Figs. 6 and 7). The range  
203 of  $\delta^{13}\text{C}_{\text{org}}$  values from the Nianduo section broadly correspond to the coeval range known from the  
204 western Tethyan Apennine and High Atlas platforms (Trecalli et al., 2012; Bodin et al., 2016).  
205 Taken together, therefore, these observations suggest that the  $\delta^{13}\text{C}_{\text{org}}$  signal from the Nianduo  
206 section is not significantly modified by diagenesis.

207 Given the abrupt facies change and appearance of coarse grained siliciclastic-rich beds at the  
208 upper Pupuga Formation to lower Nieniexionglia Formation boundary, we consider the possible  
209 influence of organic-matter source changes on our  $\delta^{13}\text{C}_{\text{org}}$  data caused by microfacies variations

210 and terrestrial input. To do this, we divided the lithologies of the Nianduo and Wölong sections  
211 into four characteristic microfacies based on grain type and/or size (Figs. 3 and 4).  $\delta^{13}\text{C}_{\text{org}}$  data  
212 from each microfacies are shown on the stratigraphic log for the two sections (Figs. 3 and 4). In  
213 addition, Fig. 5C shows cross-plots between  $\delta^{13}\text{C}_{\text{org}}$  from each microfacies in the Nianduo section  
214 and Ti, a proxy for detrital input (e.g., Kemp and Izumi, 2014). The data indicate that each  
215 microfacies type has a wide range of  $\delta^{13}\text{C}_{\text{org}}$  values, and there is no clear relationship between  
216 microfacies and  $\delta^{13}\text{C}_{\text{org}}$ . Thus, the  $\delta^{13}\text{C}_{\text{org}}$  values from the Tibetan sections are independent of  
217 changes of grain type and/or size. Overall,  $\delta^{13}\text{C}_{\text{org}}$  varies independently of Ti for each microfacies,  
218 and although microfacies 3 is typically associated with high Ti values (Fig. 5C),  $\delta^{13}\text{C}_{\text{org}}$  values of  
219 microfacies 3 are variable and show no correlation with Ti. These observations further suggest that  
220 changes in detrital input, and thus possible changes in terrestrial organic matter flux, likely have a  
221 negligible influence on the observed changes in  $\delta^{13}\text{C}_{\text{org}}$  in the Nianduo section. Nevertheless, we  
222 note that 6 samples with anomalously high  $\delta^{13}\text{C}_{\text{org}}$  values at ~10 m height in the Nianduo section  
223 come predominantly from an interval of enhanced detrital input, as indicated by higher Ti values  
224 (Fig. 3). This observation may be ascribed to the fact that these specific samples have the most  
225 significant terrigenous influence, and are thus potentially more readily affected by organic matter  
226 source change, i.e., compositional mixing. Indeed,  $\delta^{13}\text{C}_{\text{org}}$  in both sections may be sensitive to  
227 organic matter source changes given the conditions of extremely low TOC values (typically  $\ll 1\%$ ,  
228 Fig. 3). Therefore, we can reasonably infer that a few scattered and anomalously high  $\delta^{13}\text{C}_{\text{org}}$   
229 values from microfacies 1, 3 and 4 in the Wölong section may also be influenced by  
230 compositional mixing (Fig. 4).

231 5.2. The T-OAE record in the Tibetan Himalaya

232 As noted earlier, the overall  $\delta^{13}\text{C}_{\text{org}}$  trend in the Nianduo section is comparable to that  
233 recognized from well-preserved T-OAE of siliciclastic and carbonate successions elsewhere (e.g.,  
234 Kemp et al., 2005; Hesselbo et al., 2007; Hermoso et al., 2009, 2012; Trecalli et al., 2012;  
235 Sabatino et al., 2013; Figs. 6 and 7). The Tethyan Himalaya was a mature and tectonically  
236 quiescent passive margin of northern India, with smooth subsidence during the Jurassic  
237 (Sciunnach and Garzanti, 2012). Therefore, our studied Tibetan Himalayan sections can be readily  
238 correlated with each other on the basis of the characteristic top *Lithiotis* beds and associated  
239 flooding surfaces (Fig. 4). This correlation indicates that the onset of the  $\delta^{13}\text{C}_{\text{org}}$  excursion of the  
240 Nianduo section is marked by environmental and biotic changes, i.e., a sharp facies change,  
241 benthic extinction level, development of dysoxic bottom waters (Wignall et al., 2006; Han et al.,  
242 2016) and TOC increase (Fig. 3 and 4). As noted in section 2.2, we attribute these marked changes  
243 to the onset of the T-OAE owing to the biostratigraphic age constraints in the sections, and  
244 because the onset of our new  $\delta^{13}\text{C}_{\text{org}}$  excursion agrees well with the suggested correlation between  
245 the abrupt positive  $\delta^{34}\text{S}$  excursion of the Yunjia section and the  $\delta^{34}\text{S}$  excursion recorded across the  
246 T-OAE in Yorkshire, UK (Newton et al. 2011). Indeed, no other excursion in  $\delta^{34}\text{S}$  of this  
247 magnitude is recognized elsewhere in the Jurassic (Gill et al., 2011). Some debate surrounding the  
248 age assignment of the Himalaya strata exists, however. Notably, the extremely high  $\delta^{34}\text{S}$  values  
249 and anomalously low sulfate oxygen isotope values in the Yunjia section (Newton et al., 2011)  
250 suggest that the carbonate-associated sulfate  $\delta^{34}\text{S}$  ( $\delta^{34}\text{S}_{\text{CAS}}$ ) signal in this section might have been  
251 modified by diagenesis (Gill et al., 2011). However, a recent study shows that  $\delta^{34}\text{S}_{\text{CAS}}$  can  
252 withstand burial diagenesis and reliably preserve a record of ambient seawater sulfate and early

253 diagenetic redox processes (Fichtner et al., 2017). A further consideration is that a second, broad  
254 negative  $\delta^{13}\text{C}$  CIE was reported in the bottom part of the Yunjia section (~2–27 m, shaded interval  
255 on Fig. 4), which was considered as the possible characteristic T-OAE excursion due to both its  
256 shape and the occurrence of rare calcareous nannofossils higher in the section (~88 m) that were  
257 constrained to an early mid-Aalenian age (Fig. 4; Wignall et al., 2006). Given these observations,  
258 the rapid  $\delta^{34}\text{S}$  positive excursion above this  $\delta^{13}\text{C}_{\text{org}}$  negative CIE could be regarded as a possible  
259 Aalenian event (Newton et al., 2011). Further combined with additional anomalously high  $\delta^{13}\text{C}_{\text{org}}$   
260 values ( $> -27\%$ ) in the Tibetan Himalayan sections, Gill et al. (2011) also thought that the  
261 Tibetan  $\delta^{34}\text{S}$  excursion could represent a stratigraphically higher event. However, the onset of this  
262 lower CIE in the Yunjia section is not marked by any environmental and biotic changes, and if this  
263 CIE was the T-OAE then the extinction level of the *Lithiotis* bivalves would be late Toarcian,  
264 which is considered unlikely (Newton et al., 2011). In addition, according to the available  
265 biostratigraphy and chemostratigraphy, we note that: 1) the CIE between ~2 and ~27 m occurs at a  
266 position in the *Orbitopsella* foraminifera-rich horizons (Wignall et al., 2006; Han et al., 2016),  
267 which most probably indicates a late Pliensbachian age (BouDagher-Fadel, 2008); 2) it is hard to  
268 reconcile the position of ostensible mid-Aalenian calcareous nanofossils found at the base of the  
269 Nieniexiongla Formation (12 m above the Pupuga-Nieniexiongla boundary) by Wignall et al.  
270 (2006) with the position of middle-late Toarcian ammonites found in the lower Nieniexiongla  
271 Formation by Yin (2010), and 3) as discussed in section 5.1, the absolute  $\delta^{13}\text{C}_{\text{org}}$  values of the  
272 Tibetan sections broadly correspond to those of the western coeval carbonate platforms. Hence,  
273 the biostratigraphic and chemostratigraphic constraints here suggest that the age assignment of the  
274 Yunjia section by Wignall et al. (2006) is incorrect, and the Pupuga–Nieniexiongla transition does

275 indeed correspond to the onset of the T-OAE.

276 The  $\delta^{13}\text{C}_{\text{org}}$  trend of the Wölong section close to the onset of the T-OAE does not correspond  
277 well to that of the Nianduo section (Fig. 4). This difference could be due to hiatuses caused by  
278 subaerial exposure in the shallow platform environment. In addition, although the  $\delta^{13}\text{C}_{\text{carb}}$  records  
279 in the Nianduo section overall show a negative CIE around -1.5‰, its shape and magnitude are  
280 significantly different from those of the typical T-OAE CIE elsewhere (e.g., Kemp et al., 2005;  
281 Hesselbo et al., 2007; Hermoso et al., 2009, Sabatino et al., 2013, Them et al., 2017). Such a  
282 phenomenon also occurs in the  $\delta^{13}\text{C}_{\text{carb}}$  expression of the Toarcian CIE in several Toarcian  
283 shallow-water carbonate successions elsewhere (Woodfine et al., 2008; Trecalli et al., 2012).  
284 Moreover, in other marine settings, many coeval  $\delta^{13}\text{C}_{\text{carb}}$  records in bulk carbonate and belemnites  
285 from western Tethys also do not show obvious negative CIE shapes/magnitudes that match with  
286 CIEs recorded in organic matter (e.g., Hesselbo et al., 2000; Jenkyns et al., 2002; van de  
287 Schootbrugge et al., 2005; Gill et al., 2011).

### 288 5.3. Intensified storm events and extreme warmth during the early Toarcian

289 A key feature of the Toarcian CIE interval in both the Nianduo and Wölong sections is the  
290 common occurrence of coarse-grained deposits and sedimentary structures associated with  
291 high-energy conditions within the otherwise low-energy carbonate ramp environment of the  
292 Nieniexionglia Formation (see 4.2, Figs. 3 and 4). HCS/SCS and wave rippled surfaces are  
293 important storm-generated sedimentary structures formed under oscillating wave effects  
294 (Dalrymple and Hoogendoorn, 1997). Gutter casts are generally attributed to powerful  
295 unidirectional currents created during the rising and peak phases of storms (Myrow and Southard,  
296 1996). However, recent studies have shown that abundant occurrence of HCS/SCS within

297 sandstone beds that infilled gutter casts indicates that gutter erosion and rapid subsequent infill can  
298 be ascribed to offshore-directed and oscillatory-dominant combined flows during storms (e.g.,  
299 [Collins et al., 2017](#)). Therefore, the high-frequency gutter casts, HCS/SCS, and ripple marks in the  
300 studied sections clearly indicate the process of storms. Other abundant structures occurring in  
301 coarse-grained beds, like parallel laminations, climbing ripples, graded bedding and sharp erosive  
302 bases, are similar to those of turbidites formed under traction currents. However, these units  
303 cannot be clearly identified as turbidites in the Nianduo and Wölong sections because  
304 characteristic structures formed under unidirectional flow (flute casts and current ripples), as well  
305 as Bouma-style grading, were not observed.

306 Storm-related beds in the Nianduo and Wölong sections are abundant within the T-OAE  
307 interval, after maximum flooding at the Pupuga–Nieniexiongla boundary. Two earlier marine  
308 transgressions are recorded in Pliensbachian strata of the Pupuga Formation ([Han et al., 2016](#)), but  
309 storm deposits were not observed within these older transgressive sequences. This observation  
310 indicates that increased storm bed deposition/activity was independent of changes in sea level, but  
311 closely linked to the T-OAE. Similarly, geochemical and sedimentological data have emerged in  
312 recent years to indicate that many other tropical/subtropical zones over a latitudinal range of 18°N  
313 to 35°N in the northern hemisphere of the western Tethys were also influenced by frequent storm  
314 events within the T-OAE, as summarized by [Krencker et al. \(2015\)](#). These storm deposits are  
315 present in siliciclastic- and carbonate-dominated settings along the western Tethys, especially in  
316 deeper outer carbonate ramp and (hemi)pelagic environments (e.g., [Suan et al., 2013](#); [Pittet et al.,](#)  
317 [2014](#); [Krencker et al., 2015](#); [Han et al., 2016](#)). Recent work by [Izumi et al. \(2018\)](#) has also  
318 demonstrated evidence of storm activity within the T-OAE in the shallow water margin of western

319 Panthalassa. Thus, an enhanced intensity of storm events during the early Toarcian can be inferred  
320 that resulted in a basinward shift and deepening of effective storm wave base.

321 Two primary mechanisms can lead to deposition of storm beds: (1) winter storms and (2)  
322 tropical cyclones (Masselink and van Heteren, 2014). The common occurrence of storm-generated  
323 deposits in low latitudes (18–35°, Fig. 8) during the T-OAE excludes winter storms as the  
324 predominant phenomenon, because these are generated by disturbances at the boundary between  
325 warm tropical and cold polar air masses confined to mid- to high-latitudes (30–60°) (Masselink  
326 and van Heteren, 2014). By contrast, tropical cyclones are usually generated at low latitudes on  
327 both sides of the Equator by enthalpy flux from condensation of rising warm and moist air, which  
328 is essentially tied to elevated sea-surface temperature (>26.5 °C; Gray, 1968). Evidence from  $\delta^{18}\text{O}$   
329 data from brachiopods, belemnites and fish teeth from the western Tethys suggest that seawater  
330 temperature rose significantly across the T-OAE interval (4–7 °C, e.g., Gómez et al., 2008; Suan et  
331 al., 2010; Dera et al., 2011). These results support a cause-and-effect relationship between extreme  
332 warmth and increased tropical cyclones that resulted in widely distributed storm deposits along the  
333 western Tethyan margins, as suggested by Krencker et al. (2015). Recent climate models further  
334 confirm that elevated CO<sub>2</sub> concentration and sea-surface temperature can trigger more frequent  
335 and intense tropical cyclones, and also lead to a poleward expansion of storms (Emanuel, 2016;  
336 Korty et al., 2017).

#### 337 *5.4 Possible mechanisms for biotic carbonate-platform demise and delayed recovery during the* 338 *early Toarcian*

339 The correlation between the Tethyan carbonate-platform successions indicates that the top  
340 *Lithiotis* horizon in each section coincides with abrupt facies changes coincident with the onset of

341 the  $\delta^{13}\text{C}$  CIE and biotic platform demise by drowning or switching to non-skeletal carbonates (Fig.  
342 7; Trecalli et al., 2012; Sabatino et al., 2013). Based on the chemostratigraphy and biostratigraphy,  
343 the late Pliensbachian–earliest Toarcian Kioto platform was a healthy carbonate platform  
344 dominated by hyper-productive massive mound-building bivalves (*Lithiotis* group), just like other  
345 tropical Tethyan and Panthalassan shallow-water carbonate platforms during the Early Jurassic  
346 (Fraser et al., 2004; Franceschi et al., 2014). The drowning of these platforms in the early Toarcian  
347 during the T-OAE was a regional, if not global, phenomenon. Notably, in the western Tethys (Fig.  
348 8), the Pliensbachian-earliest Toarcian *Lithiotis* limestones of the NW Adriatic carbonate platform  
349 (Slovenia, central and western Croatia and western Bosnia) were directly overlain by early  
350 Toarcian dark spotted limestones (Vlahović et al., 2005; Sabatino et al., 2013), and deposits with  
351 abundant *Lithiotis* bivalves, sponge, and coral of the Djebel Bou Dahar platform were covered by  
352 Toarcian silty shale and limestones/marl alternations (Merino-Tomé et al., 2012). However, some  
353 platforms experienced transient drowning or shifted to an unfossiliferous platform type. The  
354 shallow-water carbonates rich in *Lithiotis* bivalves of the western Trento and Campania–Lucania  
355 platforms turned to clay-rich facies, and were locally replaced by crinoid-rich and unfossiliferous  
356 oolitic sediments, respectively (Woodfine et al., 2008). Several resilient platforms (Apennine and  
357 Pelagonian platforms, and the rest of NW Adriatic platform) changed from biotic platform type,  
358 dominated by *Lithiotis/P. mediterraneus*, to unfossiliferous oolitic platform (Vlahović et al., 2005;  
359 Scherreiks et al., 2010; Trecalli et al., 2012). These observations show that the demise of early  
360 Toarcian biotic platforms through either drowning or changing to fossil-scarce oolitic platforms  
361 was prevalent along the entire Tethyan tropical/subtropical realms (Fig. 8).

362 Some areas of the western Tethys were located in a relatively tectonically active area during



363 the early Toarcian, and hence tectonic subsidence could be the major factor that led to drowning of  
364 some platforms (Lachkar et al., 2009; Merino-Tomé et al., 2012). However, this process alone was  
365 unlikely to have been a significant causal influence on Kioto platform drowning in the Tethyan  
366 Himalaya because the mature passive margin of northern India was relatively tectonically  
367 quiescent, with smooth reconstructed subsidence curves through the early Jurassic (Sciunnach and  
368 Garzanti, 2012). Several meters of sea-level rise occurred during the early Toarcian at the  
369 *tenuicostatum (antiquum)–falciferum* zone transition (Suan et al., 2010, 2011). Nevertheless, for a  
370 healthy and highly productive platform, carbonate production should have been fast enough to  
371 keep up with this rise (Schlager, 1981; Godet, 2013).

372 A number of key palaeoenvironmental factors, such as nutrient excesses, anoxic/suboxic  
373 conditions, acidification, clastic delivery, elevated temperature, or a combination of these, have  
374 been suggested as potential triggering mechanisms for drowning of carbonate platforms in the  
375 geological record (Godet, 2013). Importantly, within the resolution of the  $\delta^{13}\text{C}$  data, the extensive  
376 biotic platform drowning or shifting to fossil-scarce oolitic platform occurs across the first phase  
377 of the T-OAE CIE, i.e., just before minimum isotopic values are reached (Fig. 7). The  
378 environmental deterioration of the global ocean associated with the likely large-scale release of  
379 carbon into the ocean-atmosphere system most probably led to extensive biotic platform demise.  
380 The T-OAE was associated with increased continental discharge and nutrient input (Cohen et al.,  
381 2004; Jenkyns, 2010; Brazier et al., 2015; Izumi et al., 2018). However, deeper marine shales and  
382 siltstones representing clastic input and phosphatic hardgrounds reflecting eutrophic conditions are  
383 not observed on the top of the drowning unconformity on the eastern Tethyan Kioto platform.  
384 According to detailed microfacies analysis by Han et al. (2016) and our Ti data (Fig. 3), the

385 shallow-marine carbonates are mainly overlain by lime mudstones (0–6 m) and the level of the  
386 first clastic-rich unit occurs 0.4 m above the drowning boundary. These facts indicate that there  
387 was no immediate increase in clastic delivery and nutrient input when the Kioto platform drowned.  
388 The proxies mentioned above reflecting increased clastic and nutrient input were also not reported  
389 at the boundary of the facies change in the western Tethyan Apennine and Adriatic platforms in  
390 the early Toarcian (Trecalli et al., 2012; Sabatino et al., 2013). Therefore, enhanced clastic input  
391 and subsequent eutrophication are unlikely to explain the entire Tethyan platform demise in the  
392 early Toarcian. Oxygen-depleted conditions likely influenced numerous Tethyan continental  
393 margins, because box-modeling of sulfur isotope changes suggest that pyrite burial in the NW  
394 Tethys alone could not explain the positive  $\delta^{34}\text{S}$  excursion (Gill et al., 2011). However, the mean  
395 framboid diameter distribution (5.96–8.35  $\mu\text{m}$ ) on the Kioto platform (Wignall et al., 2006) and  
396 the manganese chemostratigraphy on the Adriatic carbonate platform (Sabatino et al., 2013)  
397 suggests a sudden change from oxygen-rich to relatively lower dissolved oxygen contents in the  
398 bottom waters, which could have played a role in the abrupt demise of the Tethyan carbonate  
399 platforms. Ocean acidification also has been invoked to explain the demise of biotic platforms at  
400 the onset of the T-OAE because the prolific *Lithiotis/P. mediterraneus* are expected to be  
401 vulnerable to a reduction of carbonate saturation caused by a dramatic decrease of pH (Trecalli et  
402 al., 2012). This hypothesis seems to be reasonable on the basis of the estimated mass and rate of  
403 carbon release during the T-OAE (McElwain et al., 2005). As discussed above, extreme warmth  
404 likely prevailed along the entire tropical/subtropical Tethys through the T-OAE. Recent studies  
405 further show that a significant increase in seawater temperature, around the  
406 *tenuicostatum-falciferum* zone boundary of early Toarcian age, marks the mass extinction level

407 (Gómez et al., 2008; Gómez and Goy, 2011). Thus, warming that possibly combined with oceanic  
408 acidification and slight oxygen depletion, likely led to mass extinction of benthic fauna and biotic  
409 carbonate-platform drowning/changing to a non-skeletal platform.

410 As mentioned above, after the early Toarcian biocalcification crisis, several resilient  
411 platforms of the western Tethys quickly changed from biotic platforms, dominated by *Lithiotis/P.*  
412 *mediterraneus*, to unfossiliferous oolitic platforms, probably due to the rapid rebound of carbonate  
413 supersaturation in shallow marine environments (Vlahović et al., 2005; Scherreiks et al., 2010;  
414 Trecalli et al., 2012). If other conditions were favourable, the rapid recovery of ocean alkalinity  
415 and carbonate saturation should have promoted the thriving of biotic platforms, while  
416 unfossiliferous oolitic platforms developed extensively. Consequently, after the T-OAE biotic  
417 crisis, extreme warmth seems to have been the major factor that suppressed and postponed the  
418 recovery of biotic platforms dominated by reef-building corals or bivalves. Such a rapid and  
419 persistent warming could have triggered a severe biotic crisis, and was contemporaneously  
420 beneficial to calcium carbonate precipitation, which further facilitated the wide distribution of  
421 non-skeletal platforms in shallow settings with carbonate-supersaturated seawater. Therefore,  
422 extreme and persistent warming conditions can reasonably explain the coexistent and prevalent  
423 pattern of biotic platform demise by shifting to unfossiliferous oolitic platforms/drowning in  
424 shallow/relative deeper settings with/without carbonate-supersaturated seawater along the entire  
425 Tethys.

## 426 **6. Conclusions**

427 This study reports T-OAE records from a carbonate platform exposed in the Tibetan  
428 Himalaya, and originally deposited on the open SE Tethyan margin of the southern hemisphere.

429 Based on new biostratigraphical, geochemical and sedimentological data, we have reconstructed  
430 palaeoenvironmental and palaeoclimatic changes of the northern Indian margin through the late  
431 Pliensbachian–early Toarcian interval, encompassing the T-OAE.  $\delta^{13}\text{C}_{\text{org}}$  data from the Nianduo  
432 succession of this platform delineates the T-OAE CIE with a magnitude of  $-2.5\%$ , but a CIE with  
433 a reduced magnitude of  $-1.5\%$  is present in  $\delta^{13}\text{C}_{\text{carb}}$  data. The Wölong succession illustrates only  
434 a recovery trend in  $\delta^{13}\text{C}_{\text{org}}$  data, and not a clear CIE.

435 The common occurrence of storm deposits likely associated with tropical weather systems  
436 indicates that the well-established and marked global warming during the T-OAE severely  
437 influenced the eastern Tethyan margin. This feature of both the Nianduo and Wölong sections is  
438 similar to the observations of storm deposits made in the western Tethys of the northern  
439 hemisphere by [Krencker et al. \(2015\)](#), who also linked such storms to climate warming. The  
440 extreme warm conditions, in response to carbon release during the T-OAE, likely played a key  
441 role in the observed sudden biotic platform demise recorded in our Tibetan sections, and also  
442 observed across the wider tropical/subtropical Tethys. After the onset of the early Toarcian CIE,  
443 ocean alkalinity and carbonate saturation might have quickly recovered from the oceanic  
444 acidification, leading to conditions favorable for the extensive development of non-skeletal  
445 platforms in shallow waters ([Trecalli et al., 2012](#)). Nevertheless, the persistence of extreme warm  
446 conditions through the early Toarcian could have suppressed and postponed the redevelopment of  
447 biotic platforms dominated by reef-building bivalves and/or corals.

#### 448 **Acknowledgements**

449 We are grateful to Zhifei Liu for TOC and  $\delta^{13}\text{C}_{\text{carb}}$  analyses at the Tongji University. We thank also  
450 Wei An, Bo Zhou and Shiyi Li for their assistance in the field, and Zhicheng Huang, Yiwei Xu and

451 Weiwei Xue for their help in the laboratory, and Chao Chang, Tianchen He and Bolin Zhang for  
452 their helpful discussion. Hugh Jenkyns commented on a draft of the manuscript. We would also  
453 like to thank Editor Derek Vance, Christopher Pearce and two anonymous reviewers whose  
454 comments greatly improved the manuscript. This study was financially supported by the National  
455 Natural Science Funds for Distinguished Young Scholar in China (41525007). DBK acknowledges  
456 support of NERC Fellowship NE/I02089X/1. This is a contribution to the IGCP Project 655.

#### 457 **References**

- 458 Al-Suwaidi, A.H., Angelozzi, G.N., Baudin, F., Damborenea, S.E., Hesselbo, S.P., Jenkyns, H.C.,  
459 Mancenido, M.O., Riccardi, A.C., 2010. First record of the Early Toarcian Oceanic  
460 Anoxic Event from the Southern Hemisphere, Neuquen Basin, Argentina. *J. Geol. Soc.*  
461 *Lond.* 167, 633-636.
- 462 Al-Suwaidi, A.H., Hesselbo, S.P., Damborenea, S.E., Mancenido, M.O., Jenkyns, H.C., Riccardi,  
463 A.C., Angelozzi, G.N., Baudin, F., 2016. The Toarcian Oceanic Anoxic Event (Early  
464 Jurassic) in the Neuquen Basin, Argentina: A Reassessment of Age and Carbon Isotope  
465 Stratigraphy. *J. Geol.* 124, 171-193.
- 466 Bodin, S., Krencker, F.N., Kothe, T., Hoffmann, R., Mattioli, E., Heimhofer, U., Kabiri, L., 2016.  
467 Perturbation of the carbon cycle during the late Pliensbachian - early Toarcian: New  
468 insight from high-resolution carbon isotope records in Morocco. *J. Afr. Earth. Sci.* 116,  
469 89-104.
- 470 BouDagher-Fadel, M.K., 2008. Evolution and geological significance of larger benthic  
471 foraminifera. Elsevier, Amsterdam., vol. 404, pp. 1-544.
- 472 Brasier, M., 1990. The carbon and oxygen isotope record of the Precambrian-Cambrian boundary

473 interval in China and Iran and their correlation. *Geol. Mag.* 127, 319-332.

474 Brazier, J.M., Suan, G., Tacail, T., Simon, L., Martin, J.E., Mattioli, E., Baiter, V., 2015. Calcium  
475 isotope evidence for dramatic increase of continental weathering during the Toarcian  
476 oceanic anoxic event (Early Jurassic). *Earth Planet. Sci. Lett.* 411, 164-176.

477 Caruthers, A.H., Grocke, D.R., Smith, P.L., 2011. The significance of an Early Jurassic (Toarcian)  
478 carbon-isotope excursion in Haida Gwaii (Queen Charlotte Islands), British Columbia,  
479 Canada. *Earth Planet. Sci. Lett.* 307, 19-26.

480 Cohen, A.S., Coe, A.L., Harding, S.M., Schwark, L., 2004. Osmium isotope evidence for the  
481 regulation of atmospheric CO<sub>2</sub> by continental weathering. *Geology* 32, 157-160.

482 Collins, D.S., Johnson, H.D., Allison, P.A., Guilpain, P., Damit, A.R., 2017. Coupled ‘storm-flood’  
483 depositional model: Application to the Miocene–Modern Baram Delta Province,  
484 north-west Borneo. *Sedimentology* 64, 1203-1235.

485 Dalrymple, R.W., Hoogendoorn, E.L., 1997. Erosion and deposition on migrating  
486 shoreface-attached ridges, Sable island, eastern Canada. *Geoscience Canada* 24, 25-36.

487 Dera, G., Brigaud, B., Monna, F., Laffont, R., Puceat, E., Deconinck, J.F., Pellenard, P.,  
488 Joachimski, M.M., Durllet, C., 2011. Climatic ups and downs in a disturbed Jurassic world.  
489 *Geology* 39, 215-218.

490 Emanuel, K., 2016. Will Global Warming Make Hurricane Forecasting More Difficult? *Bull. Am.*  
491 *Meteorol. Soc.*, 495-501.

492 Fichtner, V., Strauss, H., Immenhauser, A., Buhl, D., Neuser, R.D., Niedermayr, A., 2017.  
493 Diagenesis of carbonate associated sulfate. *Chem. Geol.* 463, 61-75.

494 Franceschi, M., Dal Corso, J., Posenato, R., Roghi, G., Masetti, D., Jenkyns, H.C., 2014. Early

495 Pliensbachian (Early Jurassic) C-isotope perturbation and the diffusion of the Lithiotis  
496 Fauna: insights from the western Tethys. *Palaeogeogr. Palaeoclimatol. Palaeoecol.* 410,  
497 255-263.

498 Fraser, N.M., Bottjer, D.J., Fischer, A.G., 2004. Dissecting “Lithiotis” bivalves: implications for  
499 the Early Jurassic reef eclipse. *Palaios* 19, 51-67.

500 Fu, X., Wang, J., Feng, X., Wang, D., Chen, W., Song, C., Zeng, S., 2016. Early Jurassic  
501 carbon-isotope excursion in the Qiangtang Basin (Tibet), the eastern Tethys: Implications  
502 for the Toarcian Oceanic anoxic event. *Chem. Geol.* 442, 62-72.

503 Gómez, J.J., Goy, A., 2011. Warming-driven mass extinction in the Early Toarcian (Early Jurassic)  
504 of northern and central Spain. Correlation with other time-equivalent European sections.  
505 *Palaeogeogr. Palaeoclimatol. Palaeoecol.* 306, 176-195.

506 Gómez, J.J., Goy, A., Canales, M.L., 2008. Seawater temperature and carbon isotope variations in  
507 belemnites linked to mass extinction during the Toarcian (Early Jurassic) in Central and  
508 Northern Spain. Comparison with other European sections. *Palaeogeogr. Palaeoclimatol.*  
509 *Palaeoecol.* 258, 28-58.

510 Gansser, 1964. *Geology of the Himalayas*. Interscience Publishers John Wiley and Sons, New  
511 York (289 pp.).

512 Gill, B.C., Lyons, T.W., Jenkyns, H.C., 2011. A global perturbation to the sulfur cycle during the  
513 Toarcian Oceanic Anoxic Event. *Earth Planet. Sci. Lett.* 312, 484-496.

514 Godet, A., 2013. Drowning unconformities: Palaeoenvironmental significance and involvement of  
515 global processes. *Sediment. Geol.* 293, 45-66.

516 Golonka, J., 2007. *Phanerozoic Palaeoenvironment and Paleolithofacies Maps. Mesozoic*. *Geologia*

517 35, 589-654.

518 Gröcke, D.R., Hori, R.S., Trabucho-Alexandre, J., Kemp, D.B., Schwark, L., 2011. An open ocean  
519 record of the Toarcian oceanic anoxic event. *Solid Earth* 2, 245-257.

520 Gray, W.M., 1968. Global view of the origin of tropical disturbances and storms. *Mon. Weather.*  
521 *Rev.* 96, 669-900.

522 Han, Z., Hu, X.M., Li, J., Garzanti, E., 2016. Jurassic carbonate microfacies and relative sea-level  
523 changes in the Tethys Himalaya (southern Tibet). *Palaeogeogr. Palaeoclimatol. Palaeoecol.*  
524 456, 1-20.

525 Hermoso, M., Le Callonnec, L., Minoletti, F., Renard, M., Hesselbo, S.P., 2009. Expression of the  
526 Early Toarcian negative carbon-isotope excursion in separated carbonate microfactions  
527 (Jurassic, Paris Basin). *Earth Planet. Sci. Lett.* 277, 194-203.

528 Hermoso, M., Minoletti, F., Rickaby, R.E.M., Hesselbo, S.P., Baudin, F., Jenkyns, H.C., 2012.  
529 Dynamics of a stepped carbon-isotope excursion: Ultra high-resolution study of Early  
530 Toarcian environmental change. *Earth Planet. Sci. Lett.* 319, 45-54.

531 Hesselbo, S.P., Grocke, D.R., Jenkyns, H.C., Bjerrum, C.J., Farrimond, P., Morgans Bell, H.S.,  
532 2000. Massive dissociation of gas hydrate during a Jurassic oceanic anoxic event. *Nature*  
533 406, 392-395.

534 Hesselbo, S.P., Jenkyns, H.C., Duarte, L.V., Oliveira, L.C.V., 2007. Carbon-isotope record of the  
535 Early Jurassic (Toarcian) Oceanic Anoxic Event from fossil wood and marine carbonate  
536 (Lusitanian Basin, Portugal). *Earth Planet. Sci. Lett.* 253, 455-470.

537 Hesselbo, S.P., Pieńkowski, G., 2011. Stepwise atmospheric carbon-isotope excursion during the  
538 Toarcian Oceanic Anoxic Event (Early Jurassic, Polish Basin). *Earth Planet. Sci. Lett.* 301,



539 365-372.

540 Huang, W.T., van Hinsbergen, D.J., Dekkers, M.J., Garzanti, E., Dupont - Nivet, G., Lippert, P.C.,  
541 Li, X.C., Maffione, M., Langereis, C.G., Hu, X.M., 2015. Paleolatitudes of the Tibetan  
542 Himalaya from primary and secondary magnetizations of Jurassic to Lower Cretaceous  
543 sedimentary rocks. *Geochem. Geophys. Geosyst.* 16, 77-100.

544 Izumi, K., Kemp, D.B., Itamiya, S., Inui, M., 2018. Sedimentary evidence for enhanced  
545 hydrological cycling in response to rapid carbon release during the early Toarcian oceanic  
546 anoxic event. *Earth Planet. Sci. Lett.* 481, 162-170.

547 Jadoul, F., Berra, F., Garzanti, E., 1998. The Tethys Himalayan passive margin from Late Triassic  
548 to Early Cretaceous (South Tibet). *J. Asian. Earth. Sci.* 16, 173-194.

549 Jenkyns, H.C., 1988. The early Toarcian (Jurassic) anoxic event; stratigraphic, sedimentary and  
550 geochemical evidence. *Am. J. Sci.* 288, 101-151.

551 Jenkyns, H.C., 2010. Geochemistry of oceanic anoxic events. *Geochem. Geophys. Geosyst.* 11,  
552 1-30.

553 Jenkyns, H.C., Jones, C.E., Grocke, D.R., Hesselbo, S.P., Parkinson, D.N., 2002.  
554 Chemostratigraphy of the Jurassic System: applications, limitations and implications for  
555 palaeoceanography. *J. Geol. Soc. Lond.* 159, 351-378.

556 Kaufman, A.J., Knoll, A.H., 1995. Neoproterozoic variations in the C-isotopic composition of  
557 seawater: stratigraphic and biogeochemical implications. *Precambrian Res.* 73, 27-49.

558 Kemp, D.B., Coe, A.L., Cohen, A.S., Schwark, L., 2005. Astronomical pacing of methane release  
559 in the Early Jurassic period. *Nature* 437, 396-399.

560 Kemp, D.B., Izumi, K., 2014. Multiproxy geochemical analysis of a Panthalassic margin record of

561 the early Toarcian oceanic anoxic event (Toyora area, Japan). *Palaeogeogr. Palaeoclimatol.*  
562 *Palaeoecol.* 414, 332-341.

563 Knoll, A.H., Hayes, J.M., Kaufman, A.J., Swett, K., Lambert, I.B., 1986. Secular variation in  
564 carbon isotope ratios from Upper Proterozoic successions of Svalbard and East Greenland.  
565 *Nature* 321, 832-838.

566 Korty, R.L., Emanuel, K.A., Huber, M., Zamora, R.A., 2017. Tropical Cyclones Downscaled from  
567 Simulations with Very High Carbon Dioxide Levels. *J. Climate.* 30, 649-667.

568 Krencker, F.N., Bodin, S., Suan, G., Heimhofer, U., Kabiri, L., Immenhauser, A., 2015. Toarcian  
569 extreme warmth led to tropical cyclone intensification. *Earth Planet. Sci. Lett.* 425,  
570 120-130.

571 Lachkar, N., Guiraud, M., El Harfi, A., Dommergues, J.L., Dera, G., Durllet, C., 2009. Early  
572 Jurassic normal faulting in a carbonate extensional basin: characterization of tectonically  
573 driven platform drowning (High Atlas rift, Morocco). *J. Geol. Soc. Lond.* 166, 413-430.

574 Littler, K., Hesselbo, S.P., Jenkyns, H.C., 2010. A carbon-isotope perturbation at the  
575 Pliensbachian-Toarcian boundary: evidence from the Lias Group, NE England. *Geol. Mag.*  
576 147, 181-192.

577 Liu, G.H., Einsele, G., 1994. Sedimentary history of the Tethyan basin in the Tibetan Himalayas.  
578 *Geol. Rundsch.* 83, 32-61.

579 Masselink, G., van Heteren, S., 2014. Response of wave-dominated and mixed-energy barriers to  
580 storms. *Mar. Geol.* 352, 321-347.

581 McElwain, J.C., Wade-Murphy, J., Hesselbo, S.P., 2005. Changes in carbon dioxide during an  
582 oceanic anoxic event linked to intrusion into Gondwana coals. *Nature* 435, 479-482.

583 Merino-Tomé, O., Della Porta, G., Kenter, J.A.M., Verwer, K., Harris, P., Adams, E.W., Playton, T.,  
584 Corrochano, D., 2012. Sequence development in an isolated carbonate platform (Lower  
585 Jurassic, Djebel Bou Dahar, High Atlas, Morocco): influence of tectonics, eustacy and  
586 carbonate production. *Sedimentology* 59, 118-155.

587 Myrow, P.M., Southard, J.B., 1996. Tempestite deposition. *J. Sediment. Res.* 66, 875-887.

588 Newton, R.J., Reeves, E.P., Kafousia, N., Wignall, P.B., Bottrell, S.H., Sha, J.-G., 2011. Low  
589 marine sulfate concentrations and the isolation of the European epicontinental sea during  
590 the Early Jurassic. *Geology* 39, 7-10.

591 Oehlert, A.M., Swart, P.K., 2014. Interpreting carbonate and organic carbon isotope covariance in  
592 the sedimentary record. *Nat. Commun.* 5, 4672.

593 Pearce, C.R., Cohen, A.S., Coe, A.L., Burton, K.W., 2008. Molybdenum isotope evidence for  
594 global ocean anoxia coupled with perturbations to the carbon cycle during the Early  
595 Jurassic. *Geology* 36, 231-234.

596 Pittet, B., Suan, G., Lenoir, F., Duarte, L.V., Mattioli, E., 2014. Carbon isotope evidence for  
597 sedimentary discontinuities in the lower Toarcian of the Lusitanian Basin (Portugal): Sea  
598 level change at the onset of the Oceanic Anoxic Event. *Sediment. Geol.* 303, 1-14.

599 Sabatino, N., Vlahovic, I., Jenkyns, H.C., Scopelliti, G., Neri, R., Prtoljan, B., Velic, I., 2013.  
600 Carbon-isotope record and palaeoenvironmental changes during the early Toarcian  
601 oceanic anoxic event in shallow-marine carbonates of the Adriatic Carbonate Platform in  
602 Croatia. *Geol. Mag.* 150, 1085-1102.

603 Scherreiks, R., Bosence, D., BouDagher-Fadel, M., Meléndez, G., Baumgartner, P.O., 2010.  
604 Evolution of the Pelagonian carbonate platform complex and the adjacent oceanic realm

605 in response to plate tectonic forcing (Late Triassic and Jurassic), Evvoia, Greece. *Int. J.*  
606 *Earth Sci. (Geol. Rundsch.)* 99, 1317-1334.

607 Schlager, W., 1981. The paradox of drowned reefs and carbonate platforms. *Geol. Soc. Am. Bull.*  
608 92, 197-211.

609 Sciunnach, D., Garzanti, E., 2012. Subsidence history of the Tethys Himalaya. *Earth-Sci. Rev.* 111,  
610 179-198.

611 Suan, G., Mattioli, E., Pittet, B., Lecuyer, C., Sucheras-Marx, B., Duarte, L.V., Philippe, M.,  
612 Reggiani, L., Martineau, F., 2010. Secular environmental precursors to Early Toarcian  
613 (Jurassic) extreme climate changes. *Earth Planet. Sci. Lett.* 290, 448-458.

614 Suan, G., Nikitenko, B.L., Rogov, M.A., Baudin, F., Spangenberg, J.E., Knyazev, V.G., Glinskikh,  
615 L.A., Goryacheva, A.A., Adatte, T., Riding, J.B., Follmi, K.B., Pittet, B., Mattioli, E.,  
616 Lecuyer, C., 2011. Polar record of Early Jurassic massive carbon injection. *Earth Planet.*  
617 *Sci. Lett.* 312, 102-113.

618 Suan, G., Rulleau, L., Mattioli, E., Sucheras-Marx, B., Rousselle, B., Pittet, B., Vincent, P., Martin,  
619 J.E., Lena, A., Spangenberg, J.E., Follmi, K.B., 2013. Palaeoenvironmental significance  
620 of Toarcian black shales and event deposits from southern Beaujolais, France. *Geol. Mag.*  
621 150, 728-742.

622 Suan, G., van de Schootbrugge, B., Adatte, T., Fiebig, J., Oschmann, W., 2015. Calibrating the  
623 magnitude of the Toarcian carbon cycle perturbation. *Paleoceanography* 30, 495-509.

624 Them, T., Gill, B., Caruthers, A., Gröcke, D., Tulsy, E., Martindale, R., Poulton, T., Smith, P.,  
625 2017. High-resolution carbon isotope records of the Toarcian Oceanic Anoxic Event  
626 (Early Jurassic) from North America and implications for the global drivers of the

627 Toarcian carbon cycle. *Earth Planet. Sci. Lett.* 459, 118-126.

628 Trecalli, A., Spangenberg, J., Adatte, T., Follmi, K.B., Parente, M., 2012. Carbonate platform  
629 evidence of ocean acidification at the onset of the early Toarcian oceanic anoxic event.  
630 *Earth Planet. Sci. Lett.* 357, 214-225.

631 van de Schootbrugge, B., McArthur, J.M., Bailey, T.R., Rosenthal, Y., Wright, J.D., Miller, K.G.,  
632 2005. Toarcian oceanic anoxic event: An assessment of global causes using belemnite C  
633 isotope records. *Paleoceanography* 20, PA3008.

634 Vlahović, I., Tisljar, J., I, Maticec, D., 2005. Evolution of the Adriatic Carbonate Platform:  
635 Palaeogeography, main events and depositional dynamics. *Palaeogeogr. Palaeoclimatol.*  
636 *Palaeoecol.* 220, 333-360.

637 Wignall, P.B., Hallam, A., Newton, R.J., Sha, J.G., Reeves, E., Mattioli, E., Crowley, S., 2006. An  
638 eastern Tethyan (Tibetan) record of the Early Jurassic (Toarcian) mass extinction event.  
639 *Geobiology* 4, 179-190.

640 Woodfine, R.G., Jenkyns, H.C., Sarti, M., Baroncini, F., Violante, C., 2008. The response of two  
641 Tethyan carbonate platforms to the early Toarcian (Jurassic) oceanic anoxic event:  
642 environmental change and differential subsidence. *Sedimentology* 55, 1011-1028.

643 Xu, W., Ruhl, M., Jenkyns, H., Hesselbo, S., Riding, J., Selby, D., Naafs, B., Weijers, J., Pancost,  
644 R., Tegelaar, E., 2017. Carbon sequestration in an expanding lake system during the  
645 Toarcian Oceanic Anoxic Event. *Nat. Geosci.* 10, 129-135.

646 Yin, J.R., 2010. Jurassic Ammonites of Tibet. Geological Publishing House, Beijing (247 pp.) (in  
647 Chinese with English abstract).

648 **Figure caption**

649 **Fig. 1.** (A) Simplified tectonic map of the Tibetan Plateau showing the major blocks and sutures.  
650 MFT: Main Frontal Thrust; MBT: Main Boundary Thrust; MCT: Main Central Thrust; STDS:  
651 Southern Tibetan Detachment System; ATF: Alty Tagh Fault; KF: Karakorum Fault. (B)  
652 Geological sketch map of the Himalayas showing the studied areas, modified after [Gansser \(1964\)](#).  
653 (C) Road map showing detailed location of three Toarcian sections: Wölong, Nianduo and Yunjia.  
654 (D) Global palaeogeographic setting during the Toarcian showing the northern Indian continental  
655 margin (adapted from [Ron Blakey, <http://jan.ucc.nau.edu/~rcb7/>](#)).

656 **Fig. 2.** Field photographs of the studied sections and storm deposits within the T-OAE interval. (A  
657 and B) Nianduo section and (C and D) Wölong section showing the detailed abrupt facies change  
658 at the Pupuga–Nieniexionglā boundary (dashed white line) within the Pliensbachian–Toarcian  
659 carbonate successions. (E) Ripple marks. (F) Storm beds with HCS/SCS. (G) Sandy beds within  
660 mudstones showing weak HCS. (H) V-shaped gutter casts filled with mixed coarse carbonate and  
661 terrestrial grains showing HCS/SCS.

662 **Fig. 3.** Nianduo section shows stratigraphic distribution of organic carbon isotopes ( $\delta^{13}\text{C}_{\text{org}}$ ),  
663 carbonate carbon and oxygen isotopes ( $\delta^{13}\text{C}_{\text{carb}}$  and  $\delta^{18}\text{O}_{\text{carb}}$ ), total organic carbon (TOC), and Ti.  
664 The  $\delta^{13}\text{C}_{\text{org}}$  data are plotted as different colours based on the facies observed in thin sections of the  
665 analysed samples (microfacies 1-4 as shown in legend). Microfacies are: 1 (red datapoints):  
666 Oolitic grainstone; 2 (black datapoints): Fine-grained peloidal packstone; 3 (green datapoints):  
667 Sandy peloidal packstone/grainstone; 4 (orange datapoints): Mudstone. The red line through the  
668 data is the 3-point moving average. Note that this averaging omits the 6 datapoints (circled with  
669 blue dashed ellipse) at ~10 m height that lie well away from the rest of the data and are likely

670 influenced by terrestrial input (see main text for details). Note the distribution of storm beds and  
671 relative abundance of storm beds within the CIE interval between ~0 and ~10 m.

672 **Fig. 4.** Correlation between the Tibetan sections based on the position of the top *Lithiotis* horizon  
673 and the Pupuga–Nieniexionglia boundary, i.e., the Toarcian maximum flooding surface, facies  
674 change (Han et al., 2016) and extinction level (Wignall et al., 2006), and carbon- and  
675 sulfur-isotope stratigraphy.  $\delta^{13}\text{C}_{\text{org}}$  datapoint colour coding is based on the microfacies, as in Fig. 3.  
676 Red line through the  $\delta^{13}\text{C}_{\text{org}}$  data in both the Nianduo and Wölong sections is the 3-point moving  
677 average. Moving average for Nianduo section as in Fig. 3. For the Wölong section, 9 anomalously  
678 high  $\delta^{13}\text{C}_{\text{org}}$  values (in blue dashed ellipse) are omitted from the moving average. These are likely  
679 influenced by terrestrial input (see main text for details). The Yunjia section shows the  
680 stratigraphic distribution of organic and carbonate carbon-isotope data ( $\delta^{13}\text{C}_{\text{org}}$  and  $\delta^{13}\text{C}_{\text{carb}}$ ), and  
681 carbonate-associated sulfate (CAS) isotope data ( $\delta^{34}\text{S}_{\text{CAS}}$ ) (data from Newton et al. 2011 and  
682 Wignall et al. 2006). T-SIE: Early Toarcian sulfur-isotope excursion. Grey shading between ~2 and  
683 ~27 m in the Yunjia section delineates CIE recognised in Wignall et al. (2006), see main text for  
684 details.

685 **Fig. 5.** Cross-plots of  $\delta^{13}\text{C}_{\text{carb}}-\delta^{18}\text{O}_{\text{carb}}$  (A),  $\delta^{13}\text{C}_{\text{carb}}-\delta^{13}\text{C}_{\text{org}}$  (B) and  $\delta^{13}\text{C}_{\text{org}}-\text{Ti}$  (C) within typical  
686 microfacies of the Nianduo section. D shows characteristic microfacies 1 to 4: 1 (red datapoints):  
687 Oolitic grainstone; 2 (black datapoints): Fine-grained peloidal packstone; 3 (green datapoints):  
688 Sandy peloidal packstone/grainstone; 4 (orange datapoints): Mudstone.

689 **Fig. 6.** Chemostratigraphic correlation of the Pliensbachian–Toarcian transition from the Tibetan  
690 sections in this study with sections from Europe (Hawsker Bottoms, UK; Cohen et al., 2004;  
691 Kemp et al., 2005; Littler et al., 2010, and Peniche, Portugal; Hesselbo et al., 2007). The profiles

692 have been correlated using the onset and end of the carbon isotope excursions (CIEs). *P. spin* =  
693 *Pleuroceras spinatum*, Pl. = Pliensbachian. Note that the Wölong section does not show a clear  
694 CIE, see main text for details.

695 **Fig. 7.** Chemostratigraphic and lithological correlation of the Nianduo section with sections from  
696 the Adriatic Carbonate Platform in Croatia (Sabatino et al., 2013) and the Apennine Carbonate  
697 Platform in southern Italy (Trecalli et al., 2012). This correlation is based on the boundary of  
698 abrupt facies change from *Lithiotis* limestones to mudstones/oolitic limestones. This change is  
699 broadly consistent with the onset of the Toarcian CIE in each section.

700 **Fig. 8.** (A) Palaeogeographic map of the Tethys Ocean during the Early Jurassic showing the key  
701 locations discussed in the text (modified after Golonka (2007) and Ron Blakey,  
702 <http://jan.ucc.nau.edu/~rcb7/>). The geographic distribution of storm deposits is modified after  
703 Krencker et al. (2015). 1-Dutch Graben, Netherlands, 2-Yorkshire, UK, 3-Dotternhausen, SW  
704 Germany, 4-Sancerre core, Paris Basin, France, 5-ANDRA HTM-102 Borehole, NE France,  
705 6-Lafarge quarry, SE France, 7-Causses Basin, Central-South France, 8-Lusitanian basin, Portugal,  
706 9-Dades Valley, Morocco, 10-Bilong Co, southern Qiangtang. TCP-Trento Carbonate Platform,  
707 AdCP-Adriatic Carbonate Platform, PCP-Pelagonian Carbonate Platform, ACP-Apennine  
708 Carbonate Platform, CLCP-Campania–Lucania Carbonate Platform, DBCP-Djebel Bou Dahar  
709 Carbonate Platform, KCP-Kioto Carbonate Platform.



Fig.1

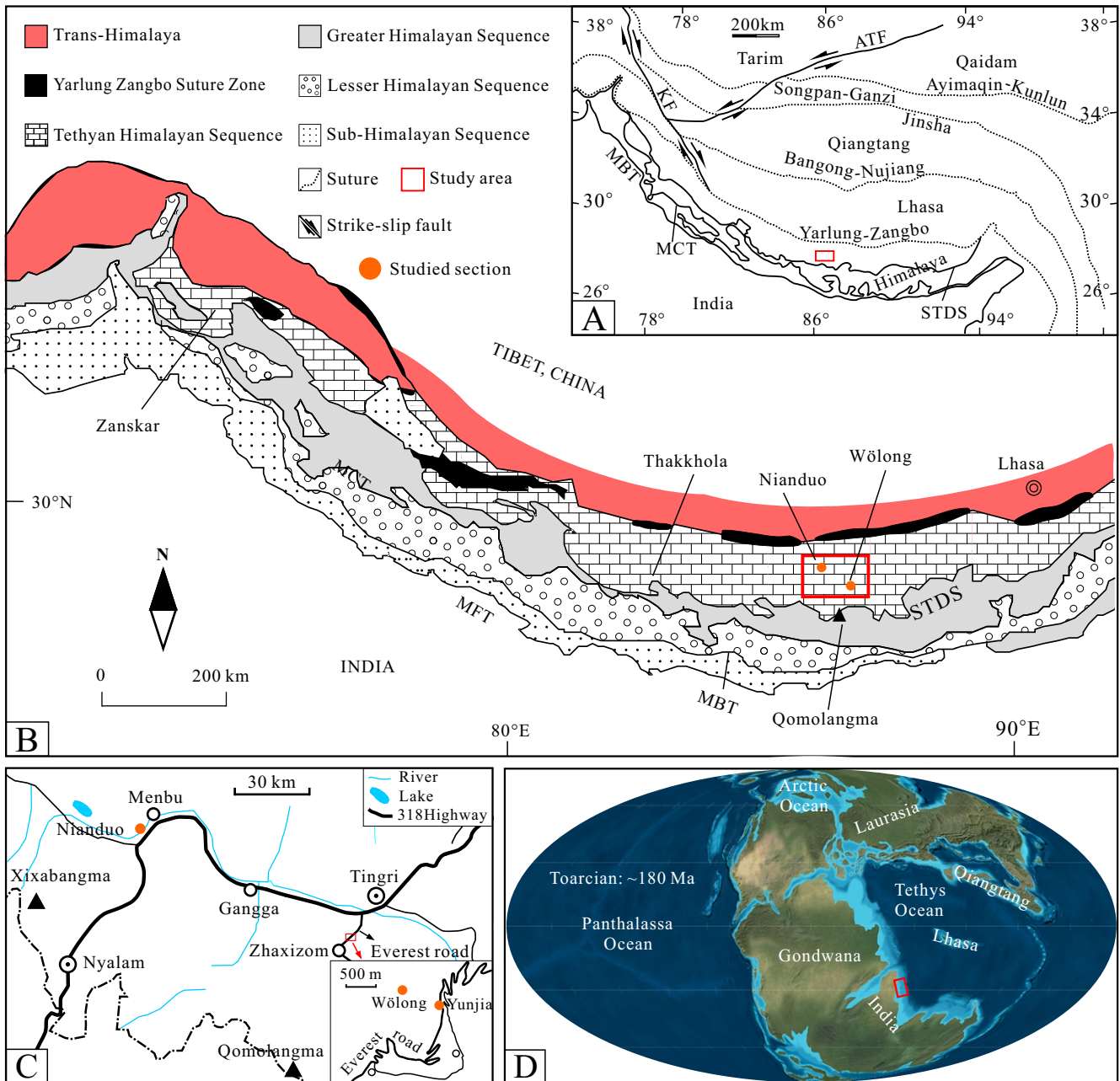


Fig.2

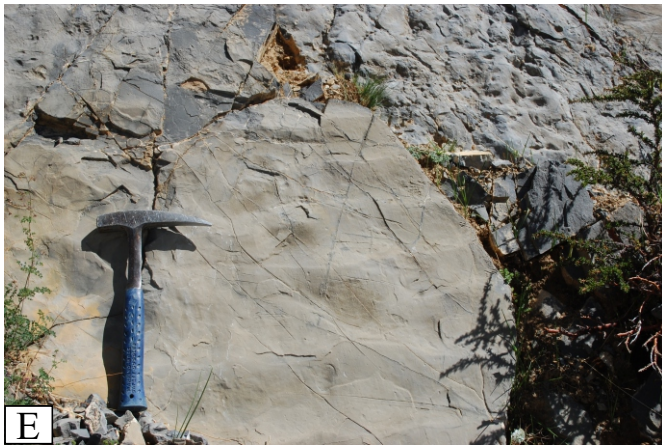
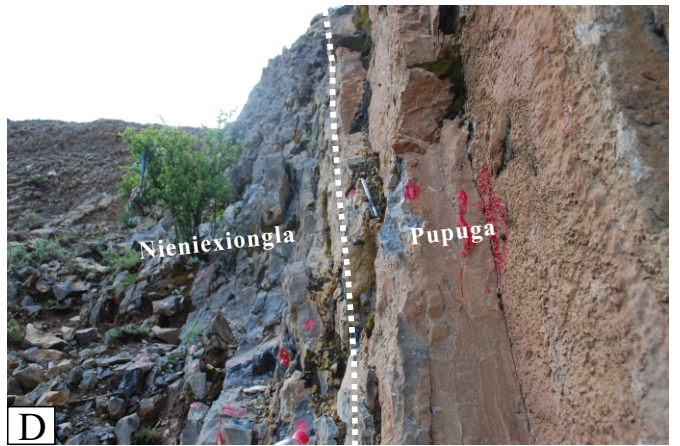
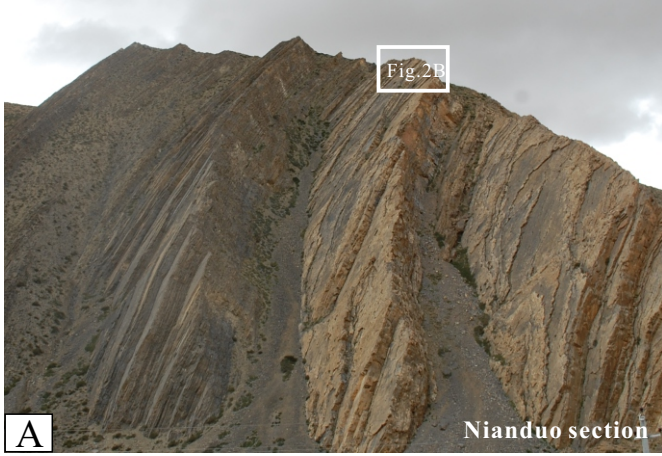


Fig.3

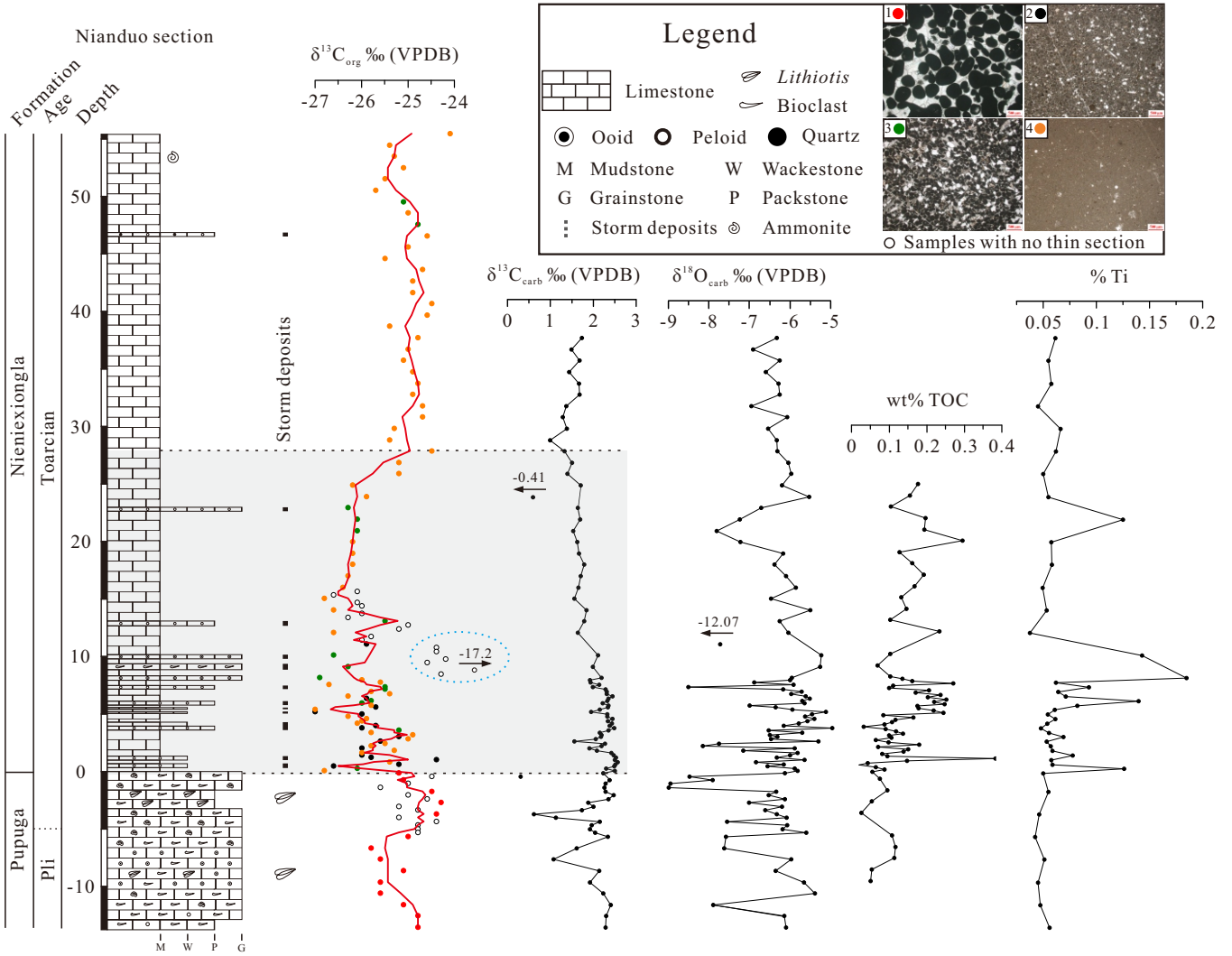


Fig.4

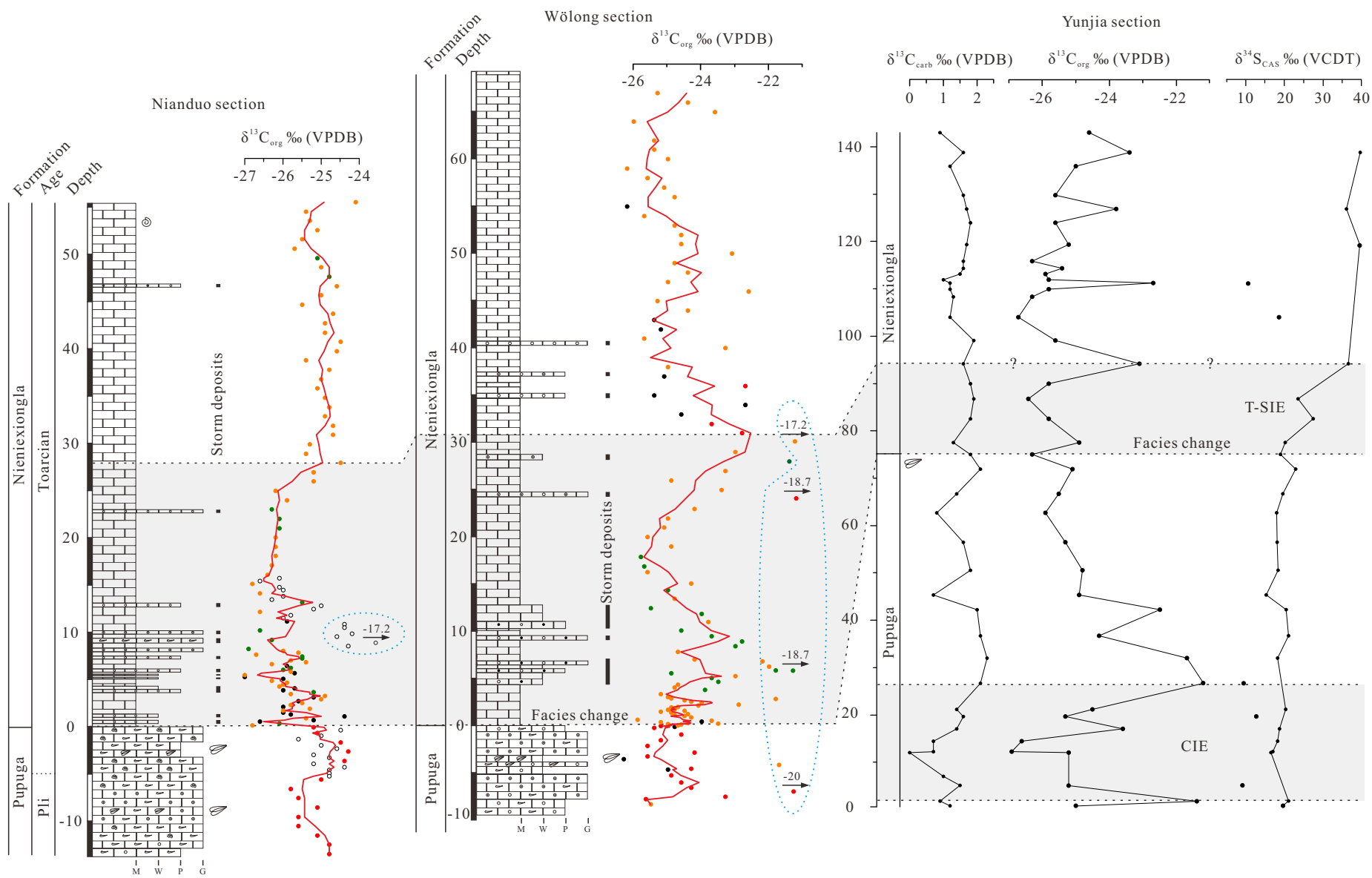


Fig.5

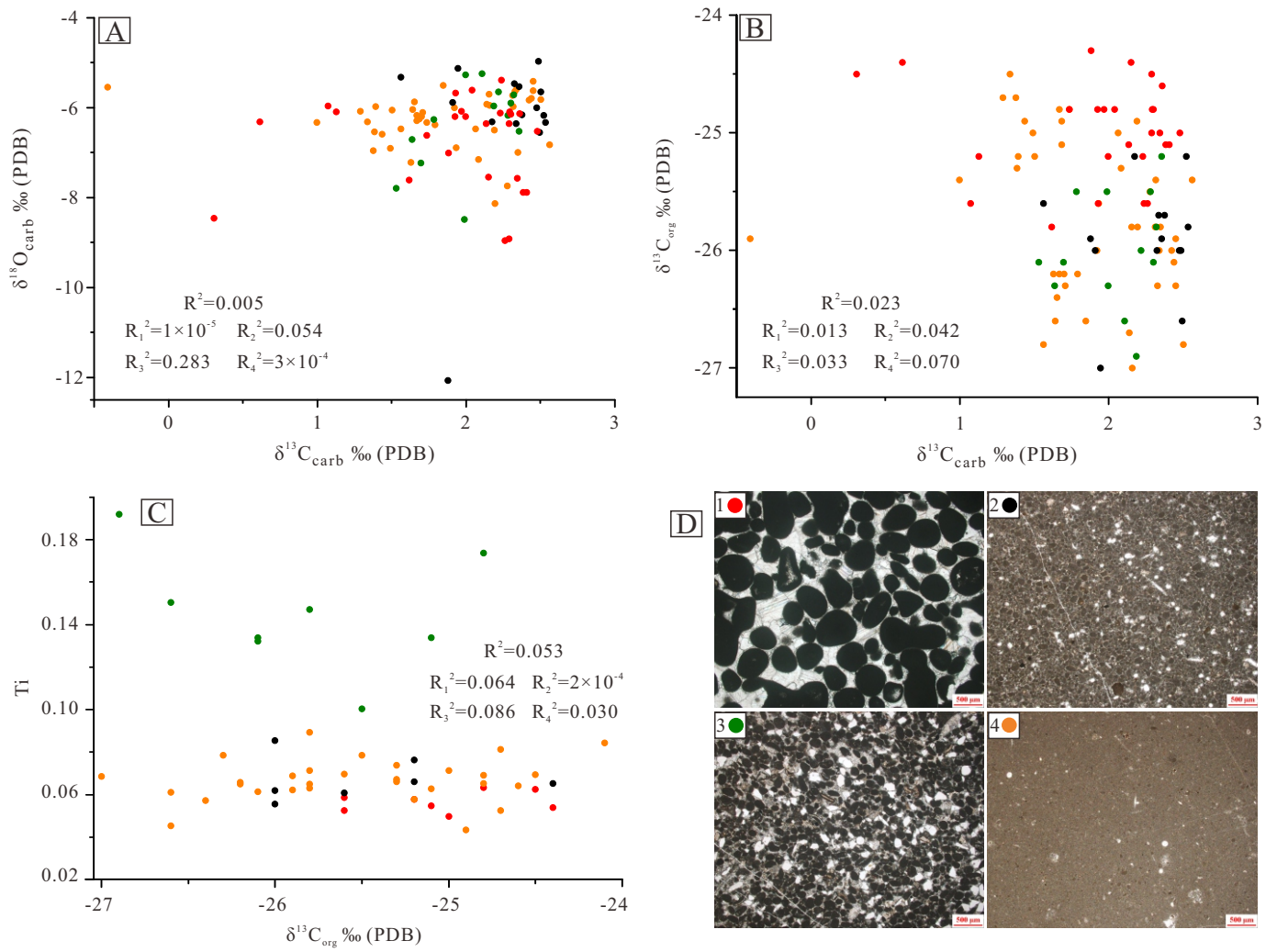


Fig.6

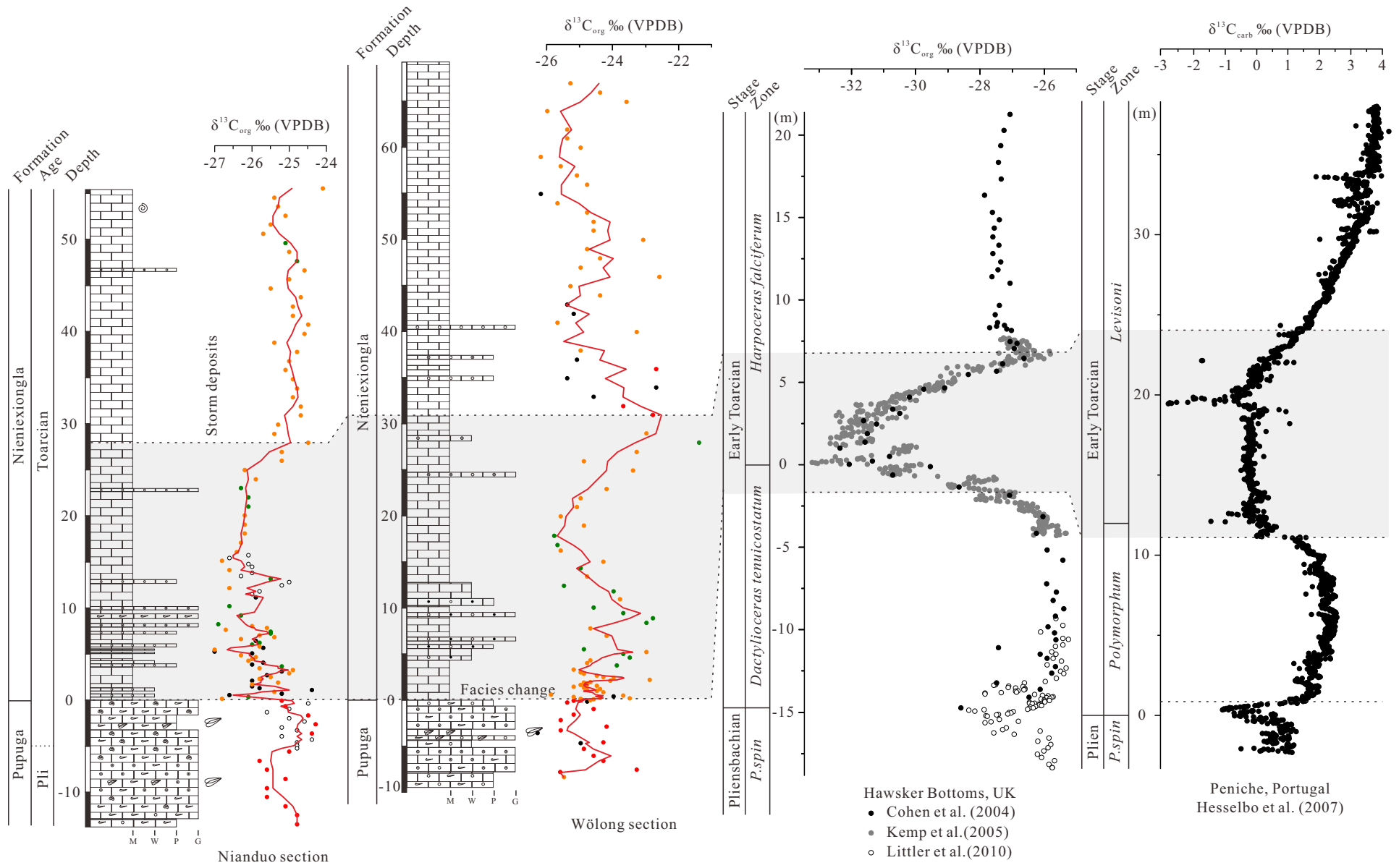


Fig.7

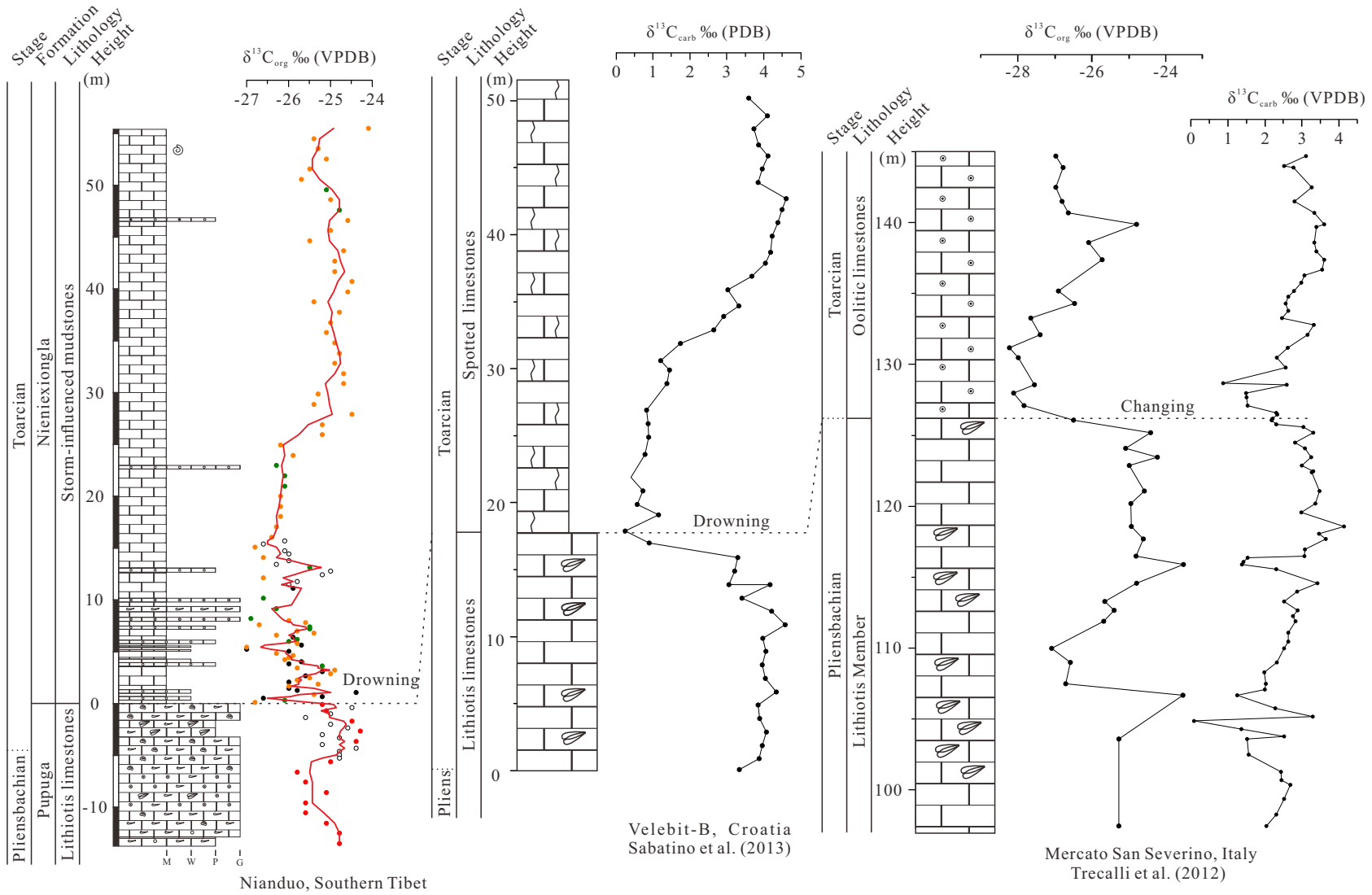
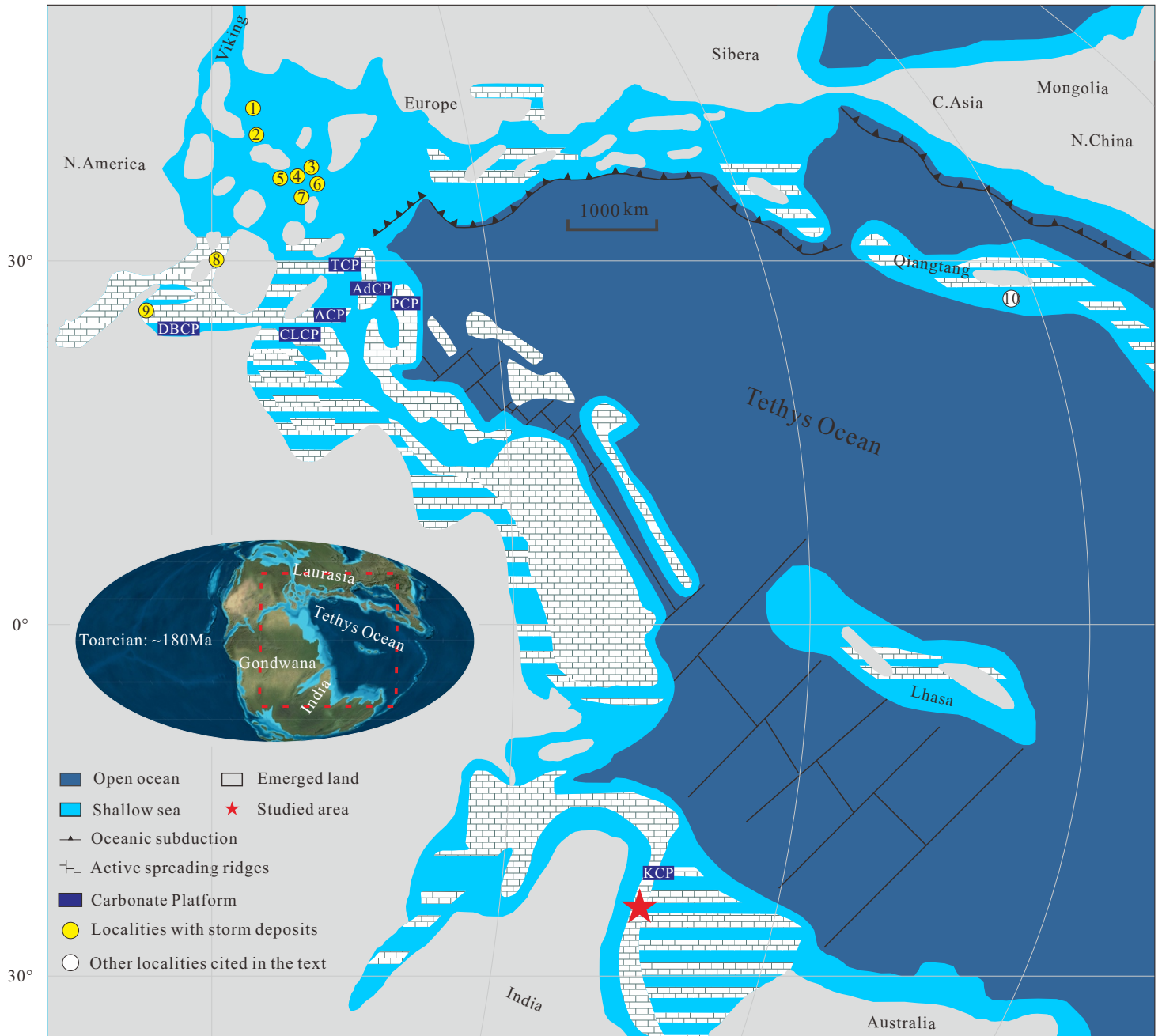


Fig.8





Raw research data (under CC BY license; see above)

[Click here to download Raw research data \(under CC BY license; see above\): Appendix.xlsx](#)